Ionospheric Simulator (IonSim): Simulating Ionospheric Conditions in a Vacuum Chamber

Saurav Dhar

Thesis submitted to the Faculty of the
Virginia Polytechnic Institute and State University
in partial fulfillment of the requirements for the degree of

Master of Science
in
Electrical Engineering

Gregory D. Earle, Chair
William T. Baumann
Scott M. Bailey

October 1, 2013
Blacksburg, Virginia

Keywords: Ion Source, Ionosphere, vacuum chamber, Low Earth orbit

Ionospheric Simulator (IonSim): Simulating Ionospheric Conditions in a Vacuum Chamber

Saurav Dhar

ABSTRACT

Understanding and improving ionospheric models is important for both military and civilian purposes. This understanding improves prediction of radio propagation used for communication and GPS navigation. Various space-borne instruments, such as retarding potential analyzers (RPAs) and ion traps are routinely flown in low earth orbit (LEO) to provide data for seeding/improve ionospheric models. This thesis describes and characterizes a new ion source that can be used to test and calibrate these space-borne instruments inside a laboratory vacuum chamber. Hot filaments are used to thermionically emit electrons inside the source. These electrons collisionally ionize neutral particles inside the source. Guided by ion-optics simulations, the ion and the electron trajectories inside the source are controlled to provide the required ion beams. A detailed description of the control electronics and the embedded controller for electron emission is discussed within. Using the custom made electronics, the source is able to provide an ion beam with current densities and mean energy comparable to the conditions in LEO.

This thesis is dedicated to my parents, without whom none of my success would be possible.

Acknowledgements

Foremost, I would like to express my sincere gratitude to my advisor Dr. Gregory Earle for his unwavering support, patience, and immense knowledge. His guidance helped me throughout graduate school and in all the time of research and writing of this thesis. I could not have imagined having a better advisor and mentor.

Besides my advisor, I would like to thank Dr. Ryan Davidson who was always there when I needed help. This thesis would not have been possible without him. Even though he does not wear his glasses often enough to look academician like, he is one of the best I know.

I thank Dr. Chad Fish for his sincere guidance and his patience. I also thank all of my committee members for their willingness to provide helpful feedback, Dr. William T. Baumann and Dr. Scott Bailey.

Last, but not least, I would like to thank Ms Chakraborti for inspiring me to expand my horizons.

Contents

List of Figures

List of Tables

Chapter 1

Introduction

1.1 What is an ion source

An ion source is an electrical or electromagnetic device that creates a beam of ions for various ground and space-based instruments such as mass spectrometers[2] and [3], particle accelerators [4], and ion engines[5]. The operating principle of a traditional ion source is simple. A conceptual cartoon of a simple ion source is shown in Figure 1.1.

One or more tungsten filaments are typically used as hot cathodes to thermionically emit electrons. These electrons collisionally ionize a fraction of the neutral atoms inside the source. With the filament directly in front of the aperture, most ions are produced near the orifice. These ions are then electrostatically accelerated in the desired direction, while simultaneously suppressing electron flux out of the source by biasing the grids that cover the aperture. A problem with this design is that the output includes photons that are created along with the thermionic electrons by the hot cathode. The output therefore gets flooded with undesirable photons that can saturate sensitive detectors placed in front of the source. A primary goal of the new design described here is to reduce this undesirable photon flux.

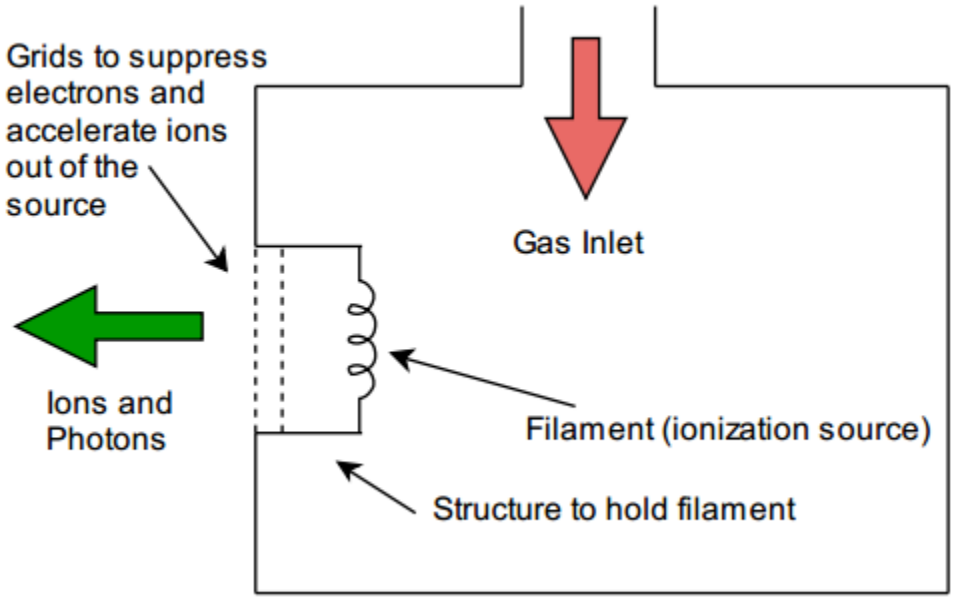

Figure 1.1: Conceptual drawing of a simple ion source

1.2 Motivation for a new ion source

Ionospheric models have been used in many aspects of geophysical research, and in understanding and improving performance of communication and positioning systems such as the global navigation satellite systems (GNSS) and the global positioning system (GPS) [6] and [7]. The spatial and temporal variations of ion temperatures, densities and relative composition are the fundamental quantities that describe ionospheric behavior. Various space-based instruments such as retarding potential analyzers (RPAs) [8] , ion traps [9] and ion drift meters [10] have been used extensively in the past to measure these important parameters.

The second goal of the proposed new ion source is to simulate some of the natural ionospheric conditions inside a laboratory vacuum chamber to provide an inexpensive platform for testing and calibration purposes. While there are various commercially available ion source systems from companies such as ULVAC, Pfeiffer vacuum and General Plasna Inc.™; they do not meet the meet the requirements needed for controlled analysis of space-borne

instruments. In addition to simulating the conditions of low earth orbit (LEO), an ideal source can be modified to simulate extraterrestrial environments, which would be useful for testing instruments built for studying the ionospheres of planets such as Venus [11] and Mars[12].

1.3 Structure of the thesis

Chapter 1 introduces the concept of an ion source and motivates the need for a new design. Chapter 2 lays down the requirements for the design, and discusses the operating principles and mechanical design of the new source. It also presents an ion optics simulation that helps to guide the new design. Chapter 3 gives a detailed description of the electronics of the source. Chapter 4 describes the embedded software that runs the electronics and presents the controller that regulates electron emission and the surface biases. Chapter 5 deals with the characterization of the output ion flux based on changes in the ion source parameters, and compares the end result with the design specs specified in Chapter 2. Finally, Chapter 6 provides a summary of main contributions of the thesis and highlights some topics for future research and development.

Chapter 2

Operating Principles of the new source

2.1 Requirements for the design

It is generally assumed that the ions in space have reached a state of equilibrium and organized themselves into a Maxwell-Boltzmann distribution, since they have had sufficient time to interact with each other and with the neutral particle background in which they are embedded. While this is very hard to achieve in a small vacuum chamber, it is desirable to have a source that can produce an ion beam with characteristics similar to that of the ions in the plasma environment that a satellite-based instrument will encounter.

An ideal source should have minimal photon flux at the output. Off the shelf solutions and the traditional ion source (Figure 1.1) have large photon fluxes at the output. When photons hit the walls of an instrument, they can cause electron emission due to the photoelectric effect, in addition to desorption of gas [13]. The desorbed gas can be ionized and the photoelectrons can multiply and accumulate in certain conditions. These factors can significantly deteriorate the beam quality and interfere with precise measurement of plasma parameters of interest.

For example, many space-borne instruments use channel electron multipliers (CEMs) to increase the signal to noise ratio, but CEMS are extremely sensitive to photons. Finally, the new source should be controllable via LabView and the output ion flux conditions should be stable and repeatable. In summary, an ideal ion source for space-science has to meet the following design specs:

1. Produce an ion beam that is similar to low earth orbit (LEO) ions in terms of relative composition, mean velocity, temperature, and density;
2. Produce minimal photon flux at the output;
3. Be controllable via LabView for ease of use;
4. Produce repeatable ion beam flux parameters over multiple uses.

Not all of these design goals can be met in a laboratory. Based on the International Reference Ionosphere (IRI) model, the relevant ionospheric conditions at midlatitudes (Latitude = 50 degrees) at a height of 400 km are given in the Table below:

Hour	Electron/Ion density (m^3)	Ion Temperature (K)
12 (Noon)	0.9404×10^{11}	1176.9
24 (Midnight)	0.4942×10^{11}	1007.1

Table 2.1: Ionospheric conditions at 400 km altititude over midlatitudes

Noon and midnight were chosen to provide the extreme conditions in the diurnal cycle. The dominant ion at this altitude is O^+, which varies between 97% to 98% of the total ion composition. Other ions at this altitude are: hydrogen (0.1% - 0.3 %), helium (0.1% - 0.2 %) and cluster ions (1.8% - 2.5 %). Maintaining a neutral atmosphere of atomic oxygen or hydrogen inside a vacuum chamber is not feasible. Moreover, it is nearly impossible to ionize helium. so nitogen is used as a proxy. We therefore try to produce an ion beam comprised of nitrogen ions with mean energy comparable to atomic oxygen in orbit.

The thermal speed of ions can be calculated by the simple relation:

$$v_{th} = \sqrt{\frac{k_B T}{m}} \tag{2.1}$$

where K_B is the boltzmann constant, T is the ion temperature and m is the mass of the ion. Based on Table 2.1, the thermal speed of the dominant O^+ ions vary between 723 m/s (midnight) and 782 m/s (noon). A satellite in circular low earth orbit at altitude 400 km will have a speed of 7670 m/s, which is much larger than the thermal speed of the O^+ ions. The maximum and minimum velocities with which a ram mounted space-borne instruments will encounter O^+ ions are 8453 m/s (7670 m/s + 783 m/s) and 6887 m/s (7670 m/s - 783 m/s), respectively. These speeds corresponds to the energies of 4.9 eV to 5.9 eV. For the source to be useful, it should produce ion beams with mean energy comparable to the above mentioned energies.

Based on the ion densities in Table 2.1, a space-borne instrument at 400 km with a circular aperture with a radius of 1.5 inches (0.0381m) is expected to collect between 0.27 μA to 0.52 μA ion current. The source must be able to produce a comparable ion current.

Moreover, the approximate pressure of the neutrals at this height is around 7×10^{-7} torr. The source must be able to operate at these pressures. The ideal design will satisfy all of these conditions, but in practice it is not possible to simulate all of these parameters simultaneously.

2.2 Mechanical Design

To meet the design criteria, a new source design named Ionospheric Simulator (IonSim) has been developed. The new source has no direct optical path for photons to the aperture. Moreover, the internal surfaces of the source are coated with a thin layer of carbon to reduce reflection of the photons. As shown in Figure 2.1, there are five main surfaces in the new

ion source design that are biased independently:

1. An aperture for the outgoing ions called the focus ring;
2. A set of four hot filament surfaces that share the same electrical bias;
3. Chamber walls;
4. Grids near the filaments;
5. A repeller surface to collect electrons and guide ions towards the aperture.

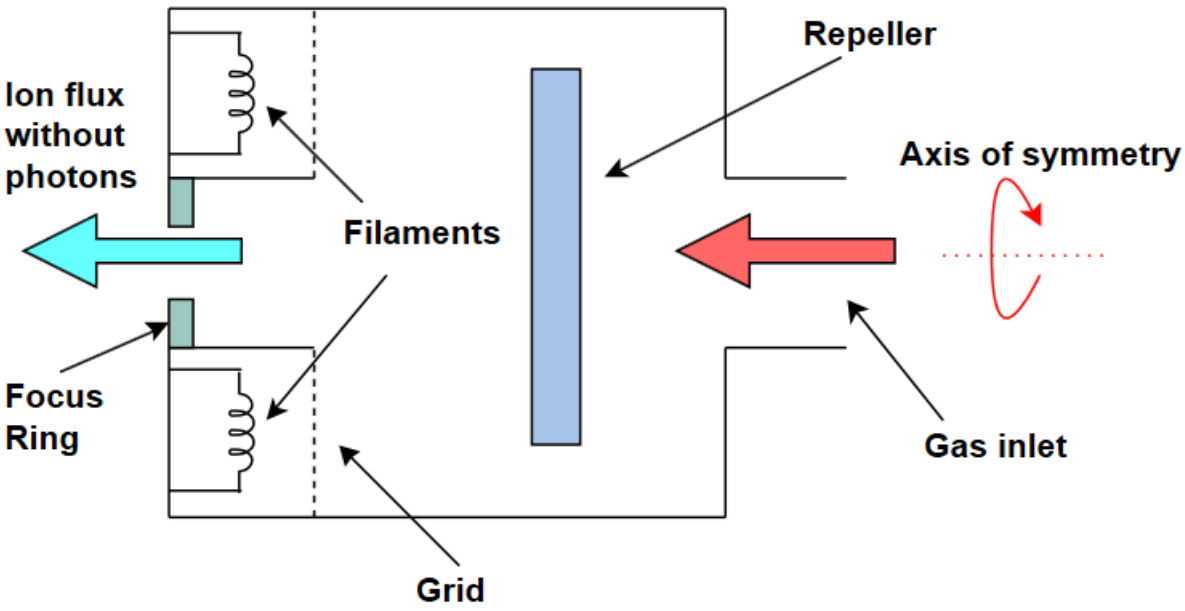

Figure 2.1: Conceptual cross section of the new cylindrically symetric ion source. Only two filaments can be seen in the cross section because the source is cylindrical and symmetric.

Figure 2.2 below shows the symetric arrangement of four filaments in a front view cutaway the cylindrical source.

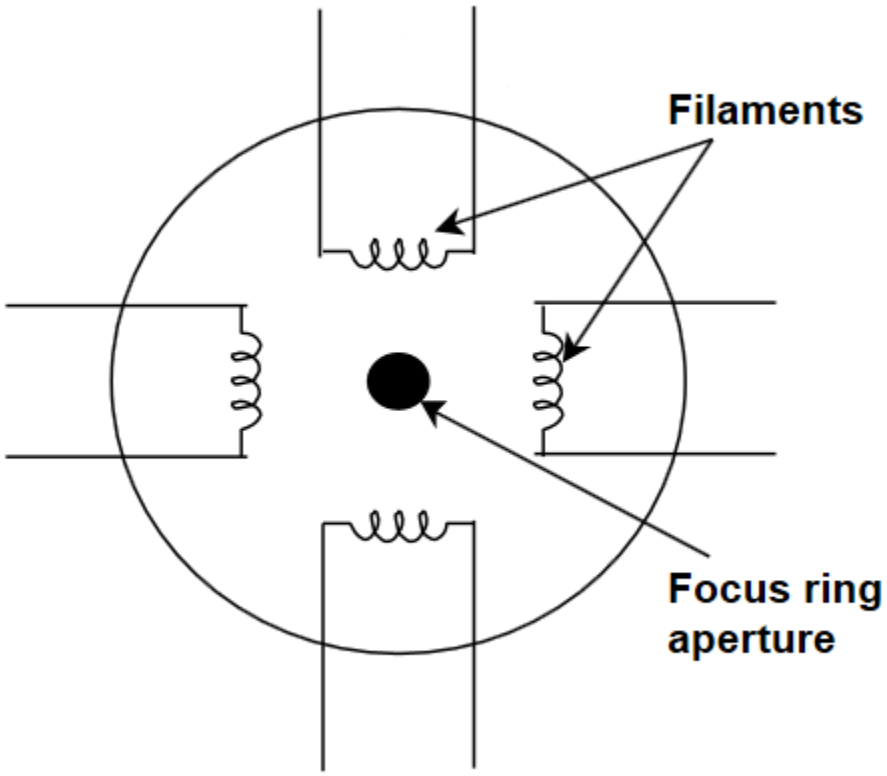

Figure 2.2: Front view cutaway of the new cylindrically symetric ion source.

First, electrons are produced at the filaments by thermionic emission. This is achieved by controlled heating of the filaments induced by a regulated current (I). The thermionic emission current density J_e can be found by the Richardson-Dushman equation:

$$J_e = A_G T^2 e^{-W/kT} \tag{2.2}$$

where, T is the temperature, W is the work function of the filament metal (normally tungsten or tungsten alloys), k is the Boltzmann constant and $A_G = \lambda_R A_0$. Where λ_R is metal specific correction and A_0 is a universal constant known as the Richardson constant and is given by:

$$A_0 = \frac{4\pi emk^2}{h^3} = 1.2 \times 10^6 A/m^2K^2 \tag{2.3}$$

Figure 2.3 below shows a typical variation of electron emission current density for tungsten based on temperature in the absence of space charges [14].

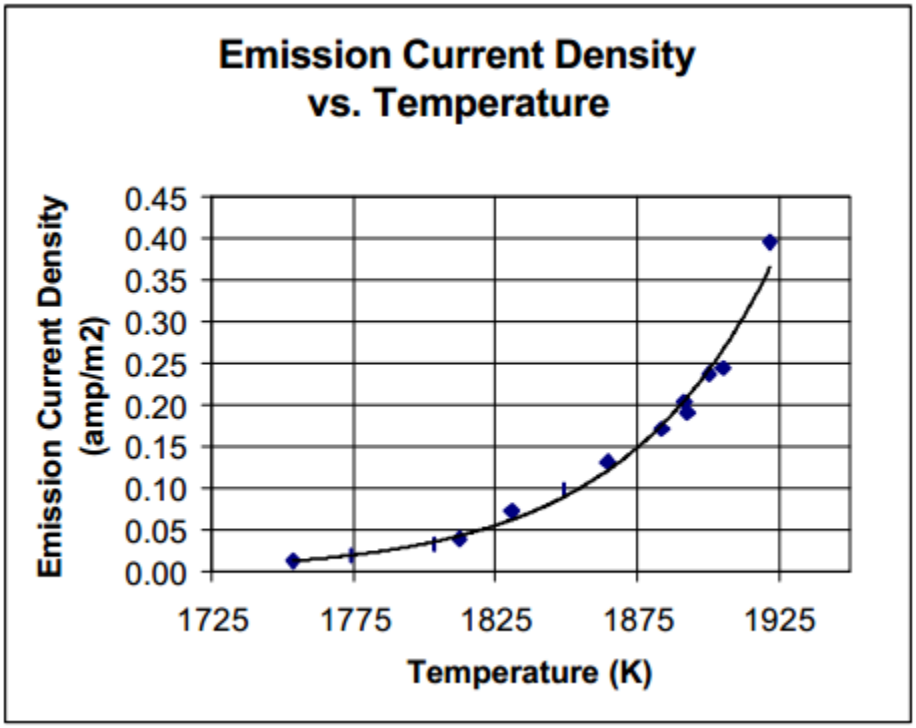

Figure 2.3: Emission current density vs. temperature in the absence of space charges for 1% Thoriated Tungsten filament. Lulai, P., 2001. Determination of filament work function in vacuum. Tech. rep., AVS, used under fair use, 2013

The relation between current passed through a filament to heat it up and the filament surface temperature can also be estimated theoretically. At steady state, the electrical power input to the filament will be equal to the conductive, convective and radiative power dissipation by the filament. This can represented by the equation :

$$I^2R = C(T - T_0) + e\sigma A_s(T^4 - {T_0}^4) \tag{2.4}$$

where I is the current passing through the filament, R is the resistance of the filament , T is the temperature of the filament, T_0 is the ambient temperature, e is the emissivity of the filament, A_s is the filament surface area, σ is the Stefan-Blotzmann constant, and C

represents the conductive and convective properties of the system. However, in near vacuum conditions, convective properties are negligible and the conductive cooling of the filaments vary depending on the filament holder geometry and materials used. A detailed thermal study of the ion source is beyond the scope of this study.

The electrons that are thermionically produced at the hot filaments are accelerated towards the repeller by adjusting voltage biases on the filaments and the grid. The chamber walls are set to a more negative voltage than the filaments to avoid collection of electrons. The grid and the focus ring are set to more positive voltages than the filament. The grid collects about 20% of the electrons emitted from the filaments and accelerates the rest towards the repeller surface. An appropriate focus ring voltage helps optimize the trajectory of these electrons. The repeller surface is strongly positive and therefore acts as the main electron sink. On the way to the repeller, the electrons collisionally ionize a fraction of the neutrals present inside the source. Since the focus ring has a negative bias, it attracts the newly produced positive ions and propels them out of the source. By varying the biases on these five surfaces, it is possible to produce an ion beam with a controllable mean energy. The composition of the ions can be varied by changing the type of gas or combination of gases at the inlet of the source. The photographs of the completed source is shown in Figures 2.5 and 2.4 .

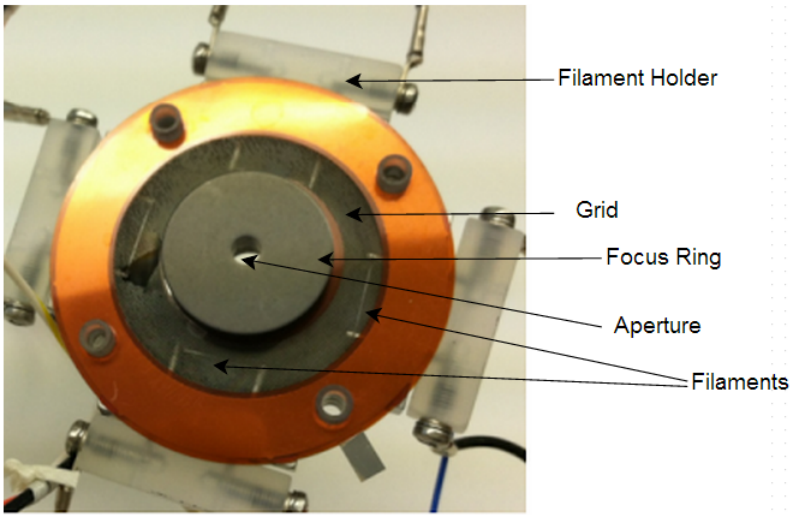

Figure 2.4: Inside IonSim - grid, focus ring and the filaments

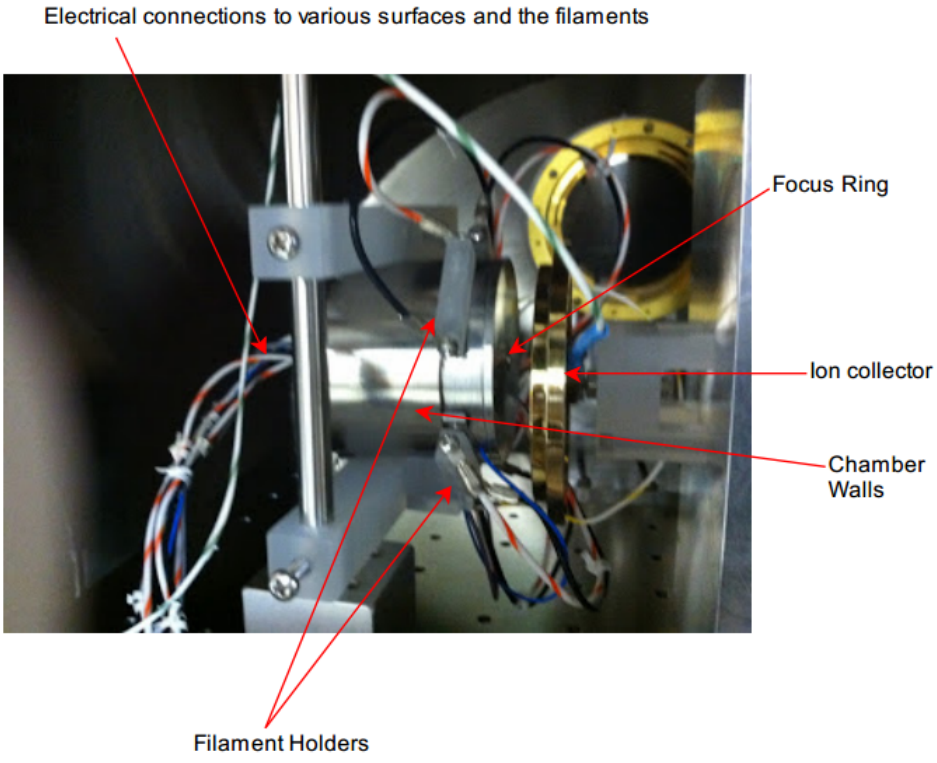

Figure 2.5: Completed ion source inside a laboratory vacuum chamber, with a collecting surface for the ions located adjacent to the aperture.

2.3 Ion Optics Simulation

Prior to building the source, ion optics simulation of the electron and ion trajectories with semi-optimized potentials on the different internal surfaces was generated by Dr. Ryan Davidson. The simulation was run using SIMION®, a software package that can be used to calculate the trajectories of charged particles in defined electric and magnetic fields. The simulation result is depicted in Figure 2.6. The red lines indicate the trajectories of the ions produced, while the black represents the electrons.

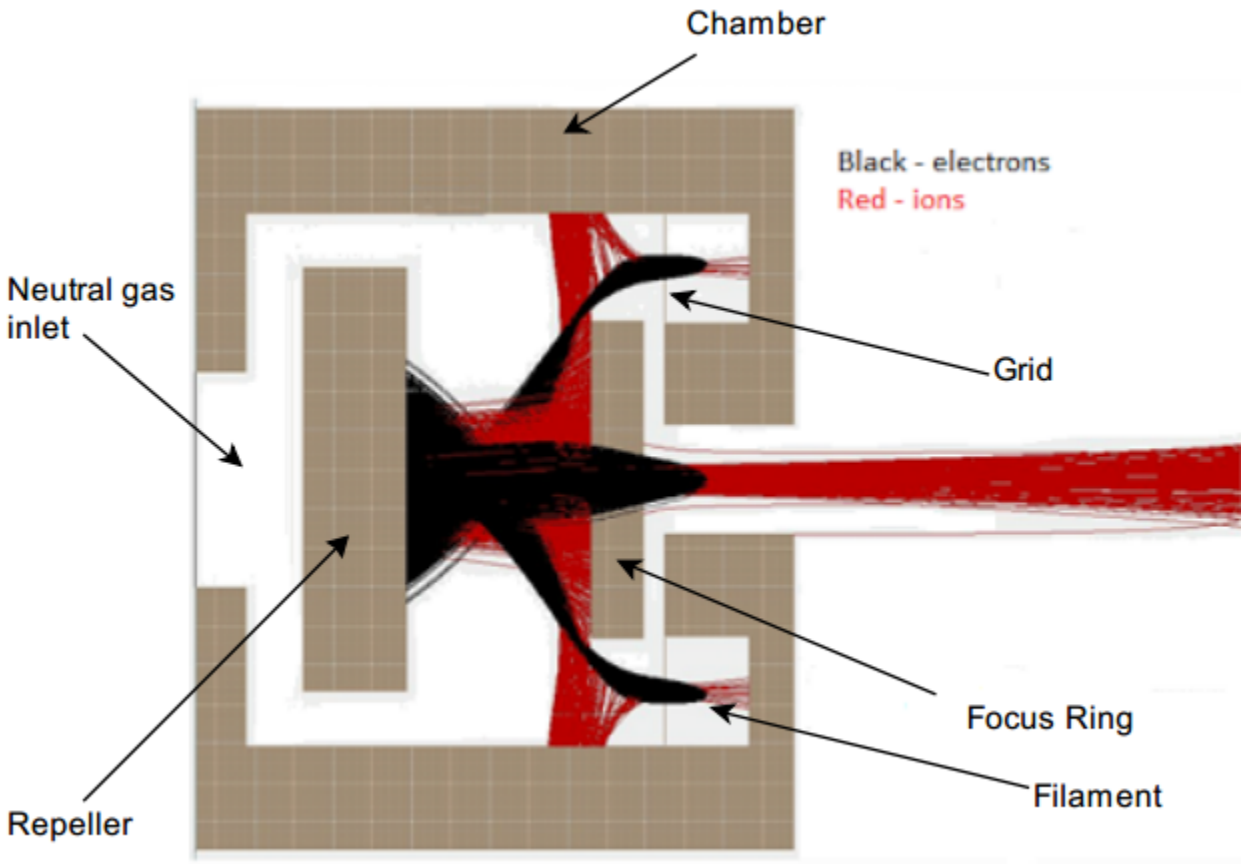

Figure 2.6: SIMION® simulation of the electron and ion trajectories inside the source. The image is used here with permission from Dr. Ryan Davidson

Once the potential gradients inside the source are mapped, the software calculates the particle trajectories with initial conditions (mass, velocity, charge and position) specified by the user. Simion® uses the relativistic Lorentz equation to calculate the forces acting on the charged particles based on the potential gradient at their position. The position of the particle is calculated after a small time interval by integrating the forces acting on it. This process of finding forces on the particle at a particular position and finding the next position based on those forces after a small time step is repeated to generate particle trajectories [15].

Table 2.2 lists the voltage biases on the different surfaces that were used to generate the potential map inside the source for the simulation result depicted in Figure 2.6.

Surface	Bias in Volts
Repeller	35
Chamber	-110
Filament	-80
Grid	-50
Focus Ring	-40

Table 2.2: Voltage biases on ion source surfaces during simulation

While the SIMION ®simulation was helpful, the algorithm that was used for this early development effort did not consider the space charge effects inside the source, which alters the performance of the device in ways that cannot be anticipated. The practical issues of space charge effects are best determined empirically. Mitigation of these effects, optimization of the output ion flux, and the design of electronics to control the source are the subjects of this thesis. The simulation results presented in table 2.2 are used as rough guidelines throughout the design and testing processes.

2.4 Particle ionization and surface potentials

The probability that a given ionization process will occur when an atom or molecule interacts with an electron is proportional to the ionization cross-section. The ionization cross-section depends strongly on the electron energy. Figure 2.7 shows the dependence of ionization cross-section on the electron energy for nitrogen, oxygen and atomic oxygen.

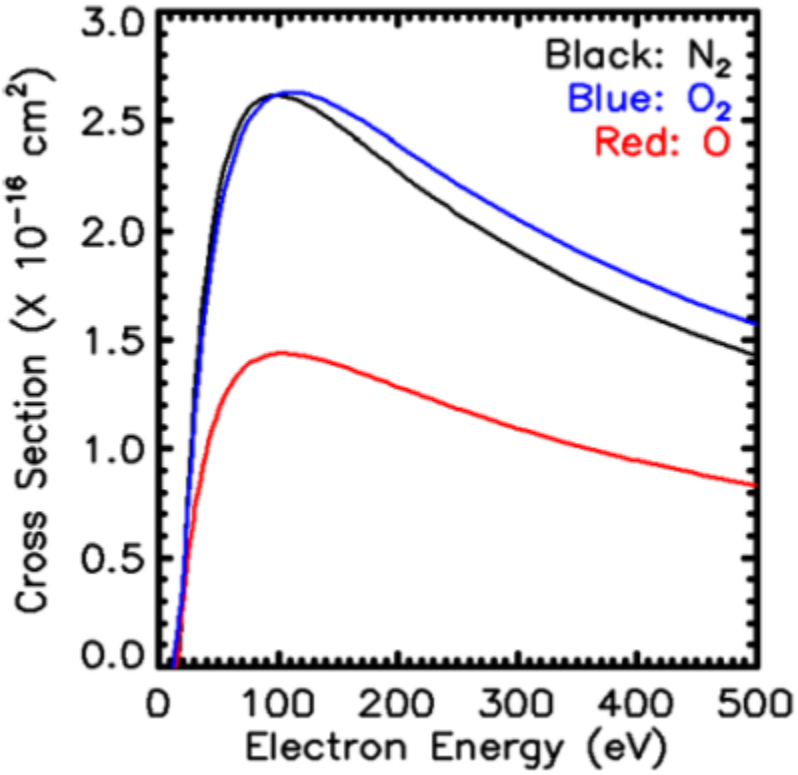

Figure 2.7: Electron impact ionization cross sections as a function of electron energy for several species. Clemmons, J. H., Friesen, L. M., Katz, N., Ben-Ami, M., Dotan, Y., and Bishop, R. L., 2012. "The Ionization Gauge Investigation for the Streak Mission". Space Science Reviews, 145(3-4), Feb., pp. 263 - 283., used under fair use, 2013

The ionization cross section for all species peaks near 100 eV, so When an electron has 100 eV of energy relative to the neutral gas it has highest likelihood of ionizing a neutral

atom or molecule. Based on the surface biases inside the source (Table 2.2), by the time the electrons reach the repeller surface they have energies of approximately 115 eV. The region of maximum ionization (i.e. the region where electrons have an energy of 100 eV) shifts based on the potentials of repeller and other surfaces inside the source. Therefore, it is very important to tweak the surface potentials so that the region of maximum ionization is in front of the focus ring and close to centerline of the device. In this way the maximum number of positive ions will be attracted toward the aperture by the focus ring, as shown in in figure 2.6.

Chapter 3

Electronics of the new source

3.1 Overall electrical control system

It is possible to use analog circuitry to control and drive the filaments in the ion source. However, the analog approach does not allow an easy way to interface the controller with a computer and is not precise or repeatable. Another method involves using commercially available programmable voltage sources with Digital to Analog Converters (DACs) and Analog to Digital Converters (ADCs) in a LabView-controlled Data AcQuisition module (DAQ). This method is expensive and bulky.

The ion source controller design described here is based on a third option that uses a dedicated microprocessor, power operational amplifiers and miniature high voltage DC-DC converters. This design is compact, relatively inexpensive, provides a surface bias of up to $\pm$ 200V inside the source and works with electron emission currents up to 200 μA per filament.

Figure 3.1 shows the overall system architecture of the IonSim. A PC running LabView is connected to the microcontroller by USB. For ease of implementation, an Arduino Mega 2560 board housing the ATmega2560 microcontroller is used as the dedicated controller in this design. The voltage biases on five independent surfaces within the source are controlled

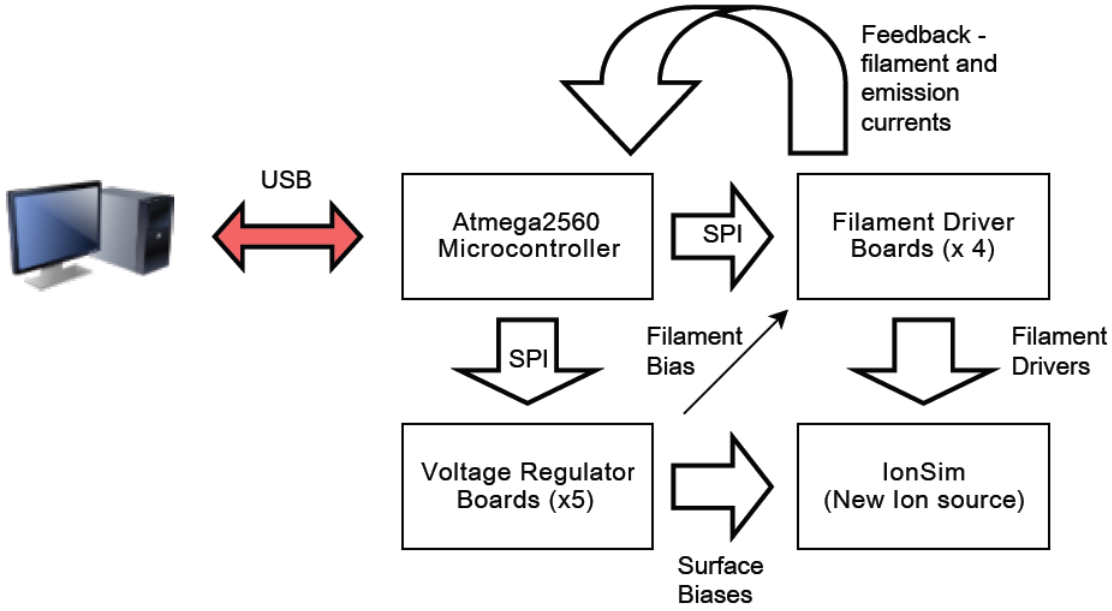

Figure 3.1: New source system architecture

by five voltage regulator boards. The ATmega2560 is connected to these voltage regulator boards via a Serial Peripheral Interface (SPI) bus. The filament driver boards, one for each of four filaments in the ion source, are also connected to the ATmega2560 by the SPI bus. In addition, the microcontroller receives real-time feedback on the status of the filament and emission currents for each of the four filaments from the filament driver boards. This helps the controller to regulate the ion emission.

The four filament driver boards and the five voltage regulator boards can independently carry out their functions, making the system very modular. Using the same boards, surface biases and electron emission by hot filaments can be controlled in this and other projects.

3.2 Voltage Regulator Boards

3.2.1 Voltage boards with single DC-DC converter

A simplified circuit diagram of a voltage regulator board containing the above components is depicted in Figure 3.2.

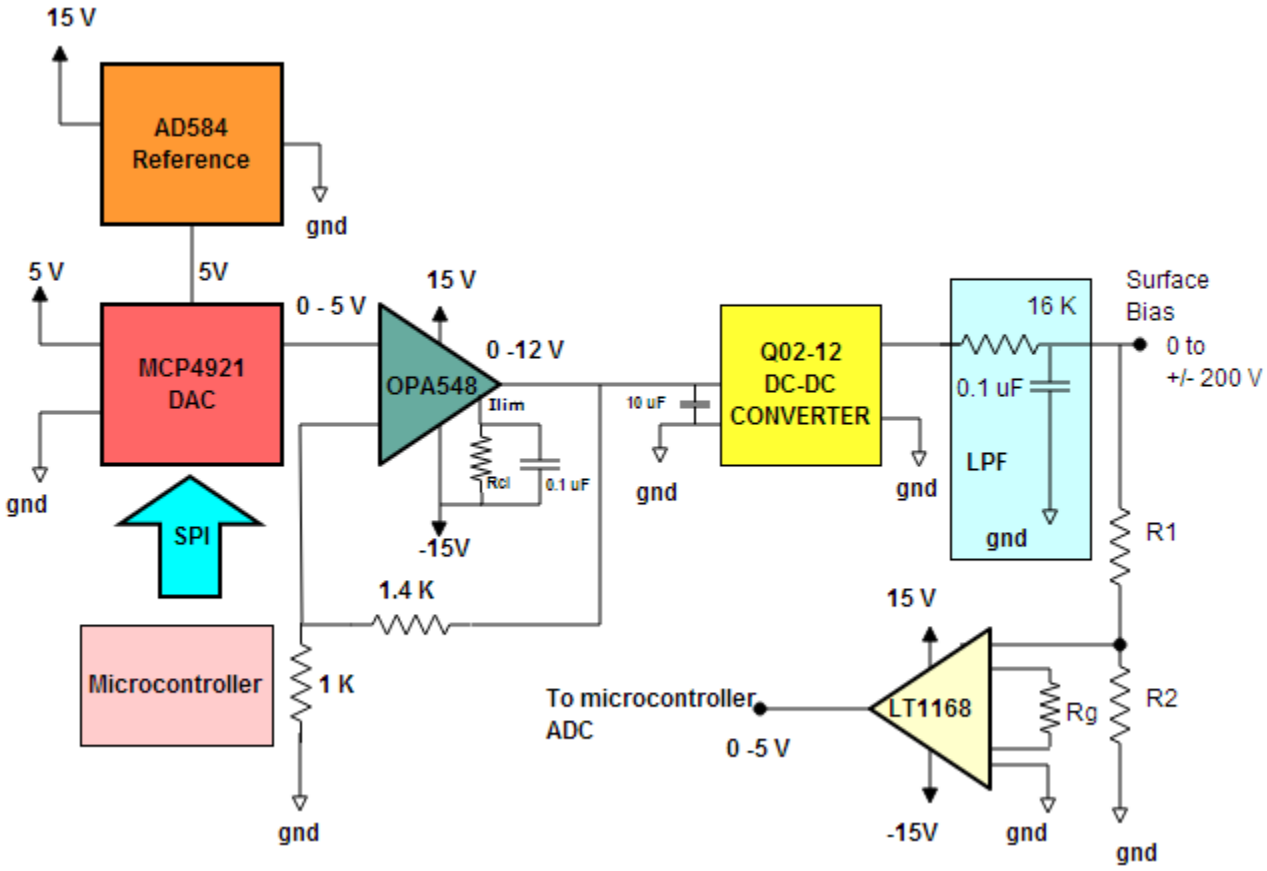

Figure 3.2: Voltage board with a single DC-DC converter

The main components of a voltage regulator board are:

1. AD584 [16] - a pin programmable precision voltage reference chip;

2. MCP4921[1] - a 12-Bit DAC with SPI interfacing capabilities;

3. OPA548T[17] - a high voltage, high current operational amplifier;

4. Q02-12[18] - a miniature 0.5W high voltage proportional DC-DC converter ;

5. Passive R-C Low Pass Filter (LPF);

6. LT1168 [19] - an instrumentation amplifier;

The dedicated reference voltage chip (AD584) on the board provides a precise 5 volt reference to the DAC, which is connected to the ATmega2560 microcontroller with a SPI interface and provides a 0-5 volt output. This output gets amplified to 0-12 volts by a non-inverting operational amplifier circuit. The output current of the power operational amplifier (OPA548) is set from 0 to 5A by the resistor R_{CL} between the I_{LIM} and the V- pins of the power op-amp. Based on the maximum output current (Max $I_O = I_{LIM}$), R_{CL} can be calculated by [17]:

$$R_{CL} = \frac{(15000)(4.75V)}{I_{LIM}} - 13750\Omega \tag{3.1}$$

A bypass capacitor of 0.1 μF is also connected in parallel to R_{CL} to attenuate noise. For the purposes of the source, the R_{CL} is set to 698 $k\Omega$ (rounded to the nearest 1% resistor value) to limit the output current to 100 mA. The output from the op-amp gets amplified further to 0 - $\pm$200 volts by the proportional DC-DC converter (Q02-12).

The output voltage of Q series DC-DC converters can contain peak to peak ripple of up to 0.25% of the output voltage at frequencies between 75-350 kHz. Therefore, a passive RC low pass filter with a cut off frequency of 1 kHz is used to nullify high frequency noise in the circuit before the output that biases the surfaces within the source. The surface bias is measured using a voltage divider circuit and a precision instrumentation amplifier - LT1168. The voltage drop across precision resistor R_2 in the voltage divider is amplified to a 0-5 V range to match the input range of the ATmega2560's internal ADC. The output impedance of the LT1168 is low ($< 100\Omega$), allowing it to act as a perfect buffer to the ATmega2560

ADC input, which is optimized for interfacing with components having output impedances of approximately 10 $k\Omega$ or less [20].

The resistor R_G is used in the LT1168 circuit to program the gain in the precision instrumentation amplifier. The value of R_G therefore depends on the desired gain G and can calculated by [19]:

$$R_G = \frac{49.4k\Omega}{(G-1)} \tag{3.2}$$

Large resistor values are used in the divider to minimize the power dissipation in the measurement circuit. Choosing a 1 $G\Omega$ resistor for R_1 and a $2.49M\Omega$ resistor for R_2 gives a maximum voltage drop across R_2 of 0.5V. A gain of 10 is required for the precision instrumentation amplifier, which makes $R_G = 5490\Omega$.

3.2.2 Voltage boards with two DC-DC converters in stacked configuration

The board described above cannot be used for biasing the surfaces that are electron sinks and are negatively biased with respect to the ground, because internal diodes limit the direction of current flow. The diode arrangement on the output pins of the Q02-12 is shown in Figure 3.3.

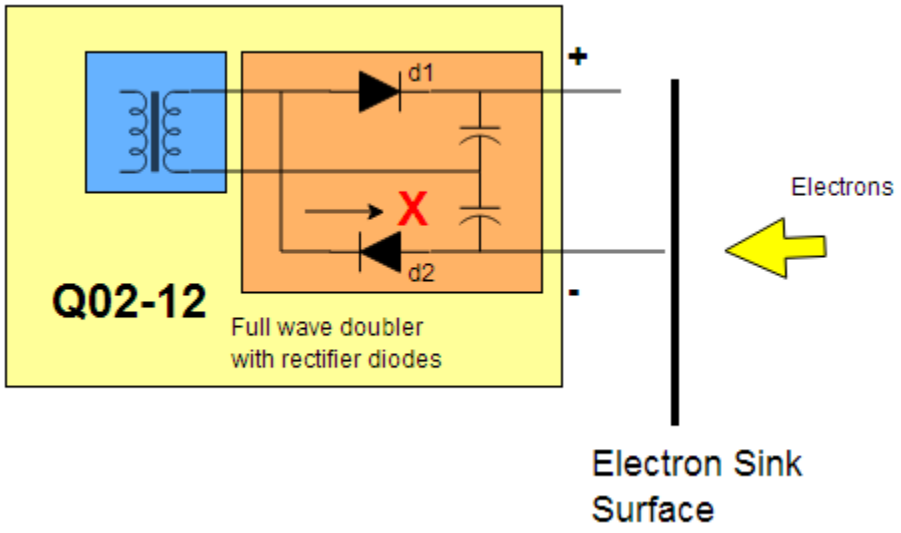

Figure 3.3: The diode configuration on Q02-12 output pins. The red "x" shows that positive current cannot flow to the negative output line.

To collect electrons while being negatively biased, positive current must be able to flow out of the negative bias pin . Due to the rectifier diode d2, positive current cannot flow out of the negative bias pin, and thus the surfaces biased negatively with this circuit cannot act as electron sinks. If electrons could not be collected on the surfaces as predicted by the ion optics simulations (see Figure 2.6), the electrons build up around the hot filaments until the hot filaments stop emitting. To rectify this space charging issue, a new design of voltage board was implemented for surfaces that must be biased negatively while acting as electron sinks inside the new source.

Two Q02-12 DC-DC converters are used in the new design. The principles of the design are illustrated in Figure 3.4. One converter floats the other converter to - 200 V. The positive output terminal of the floating DC-DC converter can then be used to bias the electron sink surface. The positive terminal can source positive current (unlike the negative terminal), and is biased negative relative to the ground as long as the floated DC-DC converter does not produce a bias of more than 200 volts between its output terminals. The bias voltage across the output terminals of the grounded converter is kept constant at 200 volts, and the bias across the terminals of the floating converter is regulated, resulting in a bias of - 200 to 0 volts with respect to ground on the positive terminal of the floating DC-DC converter.

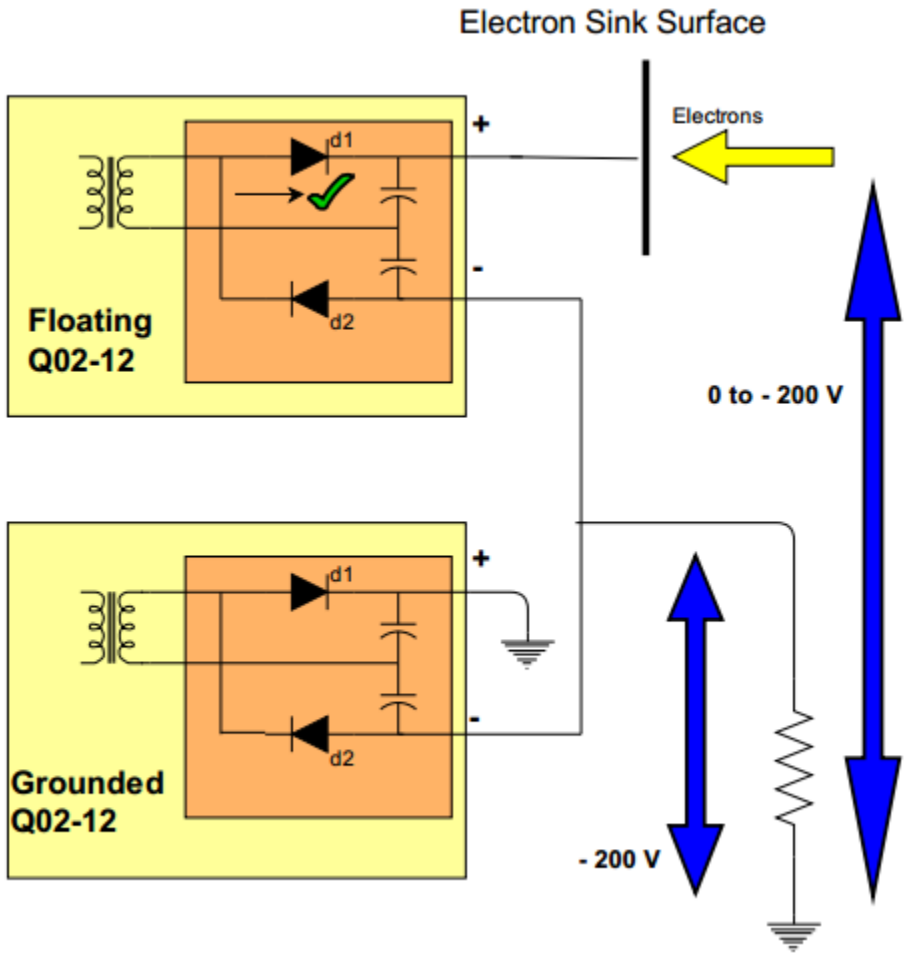

Figure 3.4: The diode configuration on Q02-12 pins

According to the ion optics simulations of the new source (Figure 2.6), the electron sinks are the grid, repeller and the focus ring. Out of these three surfaces, only the grid and focus ring need to be biased negatively (Table 2.2). Therefore the repeller, the chamber walls and the filament surfaces use the single DC-DC converter voltage boards as illustrated in Figure 3.2, while the grid and the focus ring are biased by the stacked variation as shown in Figure 3.5.

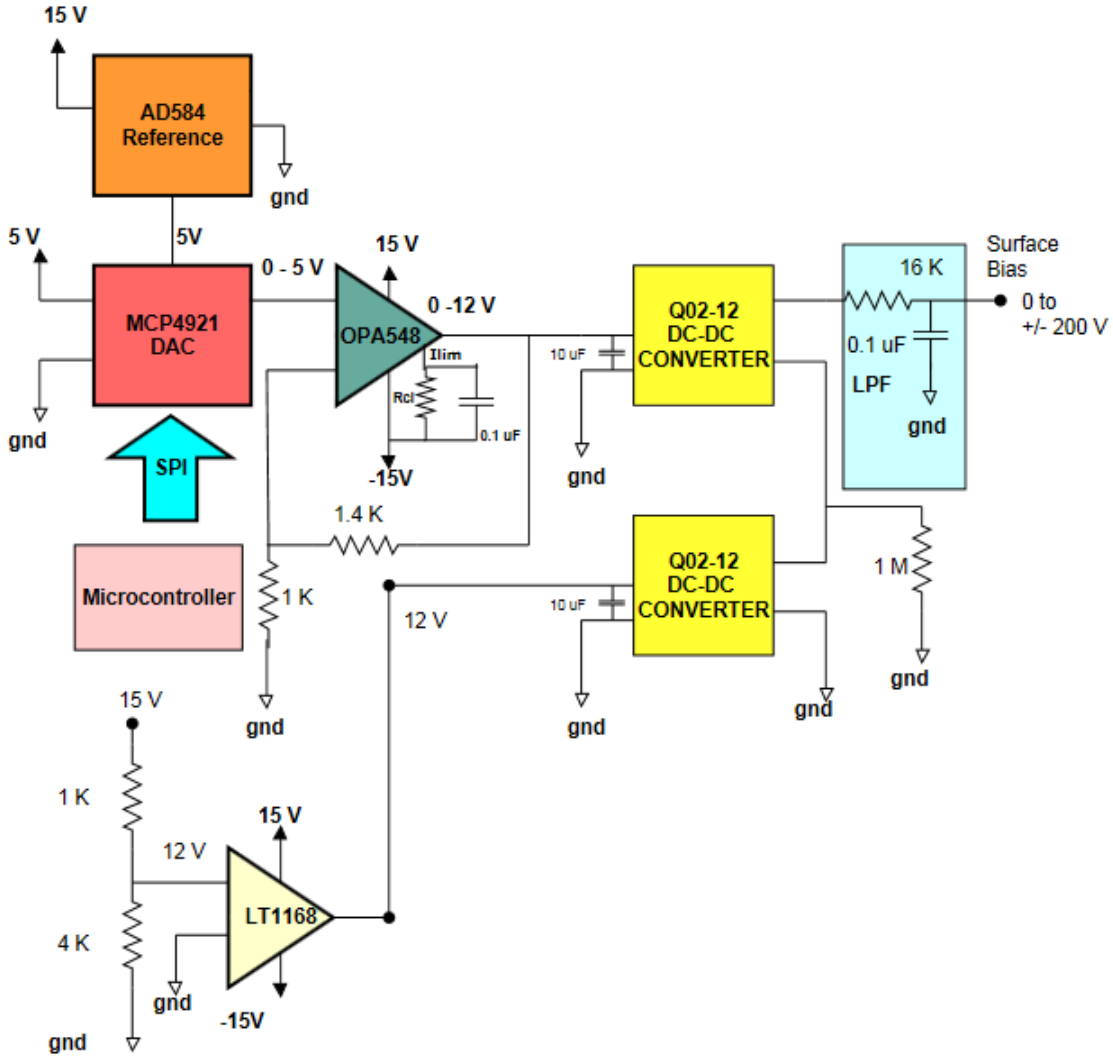

Figure 3.5: Voltage board with a double DC-DC converter

The floated DC-DC converter (the top converter in the illustration) is controlled as previ-

ously described. For the fixed DC-DC converter (the bottom one in the illustration), the 15 V supply is attenuated to a 12 V supply by a voltage divider, but the output impedance of the divider is relatively high - $Z_0 = (1K\Omega \times 4K\Omega)/(1K\Omega + 4K\Omega) = 800\Omega$ which might impact the high voltage converter [21]. Therefore, an instrumentation amplifier with unity gain is used as a buffer before the voltage is introduced to the fixed DC-DC converter. A bypass capacitor of 10 μF is used at the input pins of both DC-DC converters and the surface biases are sensed and buffered for the microcontroller ADC as previously described. The schematics for the voltage boards are presented in Appendix A.

3.3 Filament Driver Boards

3.3.1 The concept of electron emission control

The concept of electron emission control by the filament driver boards and ATmega2560 microcontroller is depicted in Figure 3.6.

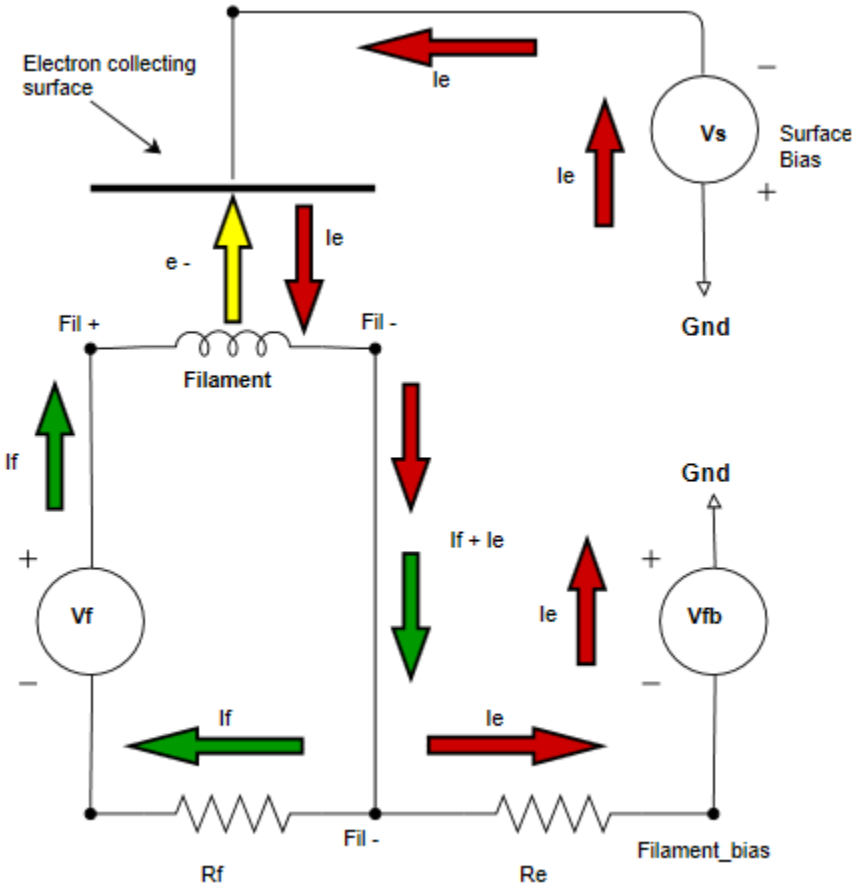

Figure 3.6: Electron emission control

For the sake of simplicity, the electron emission control for only one filament is considered here, and it is illustrated as if the emitted electrons are collected only at one surface inside the source, although in reality they are collected by multiple surfaces. Both the collecting surface and the filament are biased negatively with respect to ground, and the filament is

more negatively biased than the electron sink, $|V_{fb}| > |V_s|$.

To induce thermionic emission, a controlled voltage V_f is applied, which in turn induces a controlled current I_f and heats up the filament. With the electrons leaving the filament surface, it can be treated as a node that receives the positive emission current I_e (by convention). In Figure 3.6 the emission current I_e is shown in red, the filament heater current I_f is shown in green, and the electron emission is shown in yellow. Two precision resistors, R_f and R_e are used to sample the filament current and emission current. The voltage drops across these resistors are then amplified by precision amplifiers and is acquired by the dedicated microcontroller's internal ADC. Using the emission current I_e as feedback, the ATmega2560 uses a control scheme to stabilize the current I_f through the filament.

3.3.2 Driving the filament

Much like the voltage board, the DAC is connected to the ATmega2560 by a SPI bus and gets a 5V reference voltage from a dedicated AD584 precision voltage reference chip on the filament driver board. The DAC provides a control signal of 0-5V to the power amplifier (OPA549) that drives the filament as illustrated in Figure 3.7.

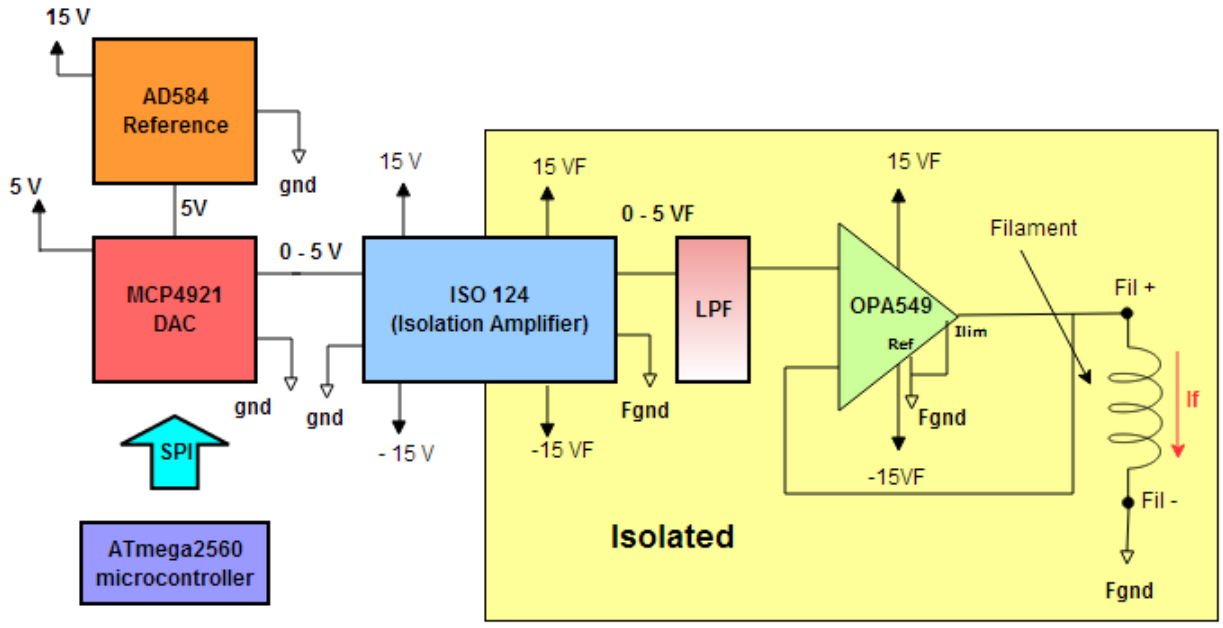

Figure 3.7: Circuit diagram for the filament driver

Based on the output of the power amplifier, a voltage difference is induced between Fil+ and the Fgnd terminals. Current through the filament is controlled by regulating this voltage difference from the microcontroller. The power amplifier is capable of driving continuous currents of up to 8A [22]. In the configuration shown in the figure above, the I_{LIM} and the Ref pins of the op-amp are connected together. This gives the power amplifier a maximum current output limit of (8A). This current limit can be altered by introducing a resistor R_{CL} between the I_{LIM} and the Ref pins to make a fail-safe mechanism to protect the filaments from overheating, as described later in this chapter.

3.3.3 Sensing the filament and the emission currents

As illustrated earlier in the electron emission control figure (Fig 3.6), the emission and the filament current are measured as voltage drops across two precision resistors, R_f and R_e. The circuit diagram for sensing the filament and emission currents is given below in Figure 3.8.

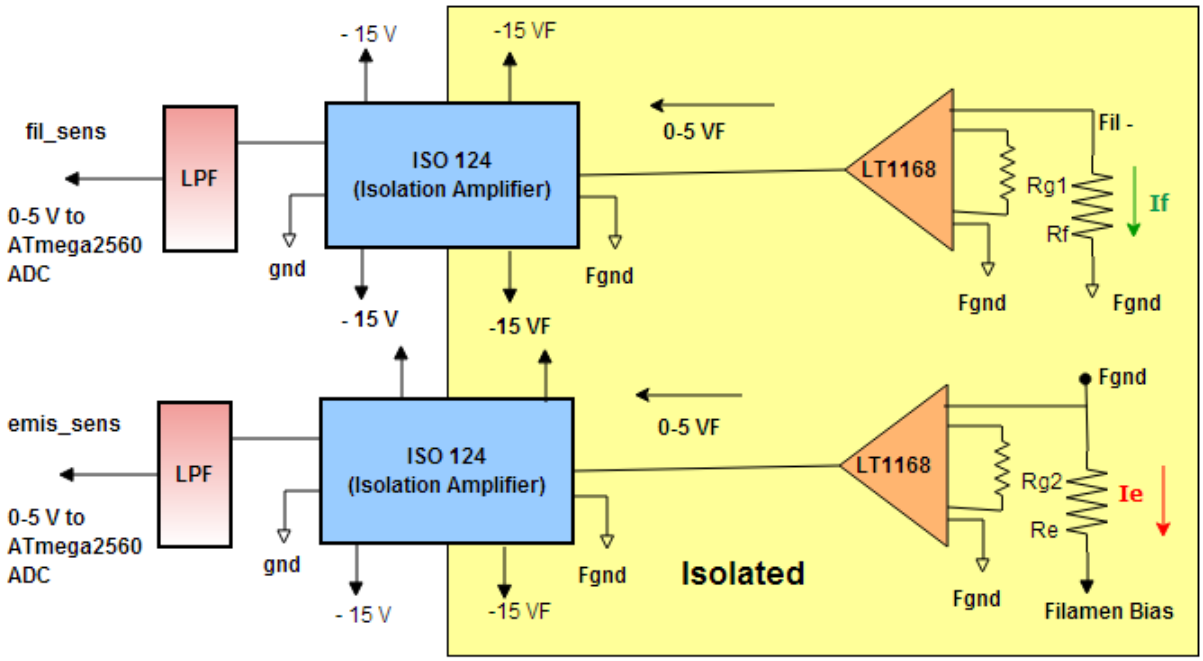

Figure 3.8: Sensing the filament and the emission currents

The filament current is sensed by the precision resistor R_f (0.05 Ω) which produces a signal (voltage drop) of approximately 50 mV/A. . The emission current is detected with the precision resistor R_e (100Ω) which produces a voltage drop of 0.1 mV/μA. The ADC of the ATmega2560 accepts a range of 0-5 V, so the voltage drops are scaled by the amplifiers to this range. The voltage drop across R_f is amplified 50 times and the voltage drop across R_e is amplified 250 times with a programmable precision instrumentation amplifier (LT1168). The amplification resistors (R_{G1} and R_{G2}) are responsible for programming the gain on the instrumentation amplifier. Their values can be easily calculated from Equation 3.2, and in

this design are set to 1 $k\Omega$ and 200 Ω respectively (the nearest 1% resistor values are used). Both these signals are passed through a low pass filter with a cut-off frequency of 1 kHz before being fed into the microcontroller ADC.

3.3.4 Isolation of the filament

Since the filament is floating relative to ground, all the connections to and from the filament are isolated with an ISO124 isolating amplifier (Figures 3.7 and 3.8). A very similar design was used by Eli Flaxer for a programmable smart hot filament electron emitter [23]. That design was modified to suit the purposes of the IonSim.

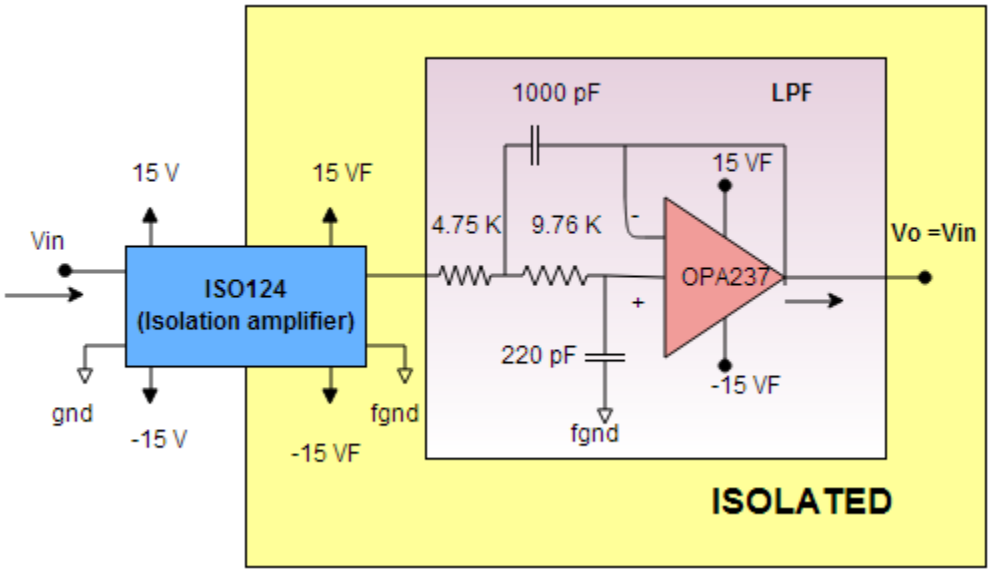

Figure 3.9: The output filter and the π filter at the power supply on ISO124 amplifiers

The ISO124 isolation amplifier is rated for a continuous isolation voltage of 1500 Vrms, therefore it can easily withstand the 200 V (maximum) difference between the microcontroller and the filament side in IonSim. The input and the output sections of the isolation amplifier are isolated by internal 1pF isolating capacitors. The input signal V_{in} is modulated and transmitted digitally across the digital barrier to the output side where it is converted back to an analog signal and the ripples inherent in demodulation are removed. However, a small 500 KHz residual demodulator ripple of 20 mV p-p remains at the output [24]. A simple 2 pole Sallen-Key type low pass filter with a 100 KHz cut off frequency using a precision op-amp (OPA237) can be added to eliminate the output ripple. The details of the filter are

shown in Figure 3.9.

This two pole low-pass filter can be added on all outputs of the isolation amplifier in both directions - for signals being fed into the isolated filament side and signals coming out of the isolated filament side. In addition to attenuating high frequency noise, these filters improve the output impedance. This helps immensely while feeding the buffered 0-5V DC signals that represent the filament and the emission currents to the ATmega2560 ADCs.

3.3.5 Sensing the need for filament replacement

In addition to sensing the filament current and the emission current , the voltage across the filament can be easily sensed with the circuit shown in Figure 3.10:

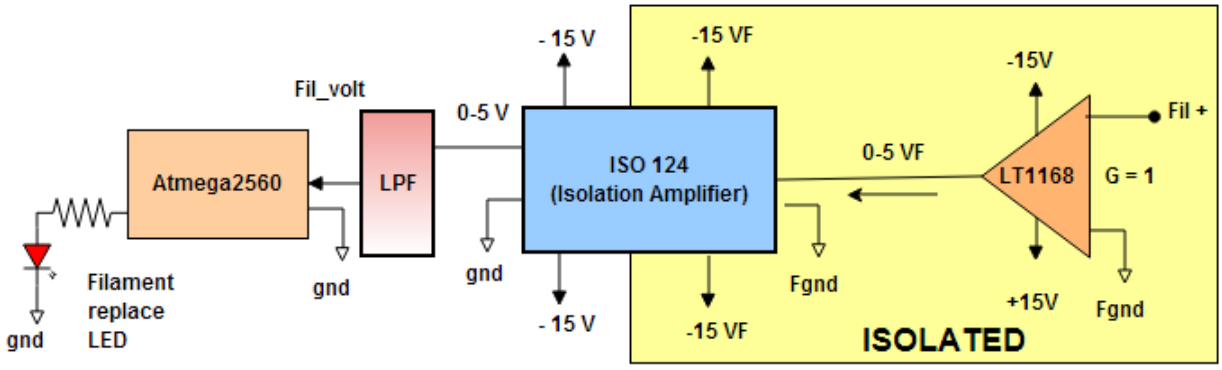

Figure 3.10: Sensing the voltage across the filament

Since the the current through the filament is also sensed, the resistance of the filament can be determined by the relation:

$$R_{filament} = \frac{V_{fil}}{I_{fil}} - R_f \tag{3.3}$$

Where V_{fil} is the sensed voltage between the Fil+ and Fgnd nodes in the circuit above, I_{fil} is the sensed current through the filament and R_f is the resistance of the precision resistor across which the filament current is sensed. Before a filament burns out its resistance increases significantly. This resistance change can be monitored by the embedded microcontroller, and a user can be notified by a blinking LED when the resistance drops below a predetermined threshold resistance. The threshold resistance will change depending on the type of filament used and its usage history.

3.3.6 Programmable protection of the filaments from overheating

The continuous output current limit of the filament driving amplifier(OPA549) can be set from 0 to 8A by controlling the input to the I_{lim} pin on the amplifier. The current limit through the filaments can be digitally controlled by the circuit shown below:

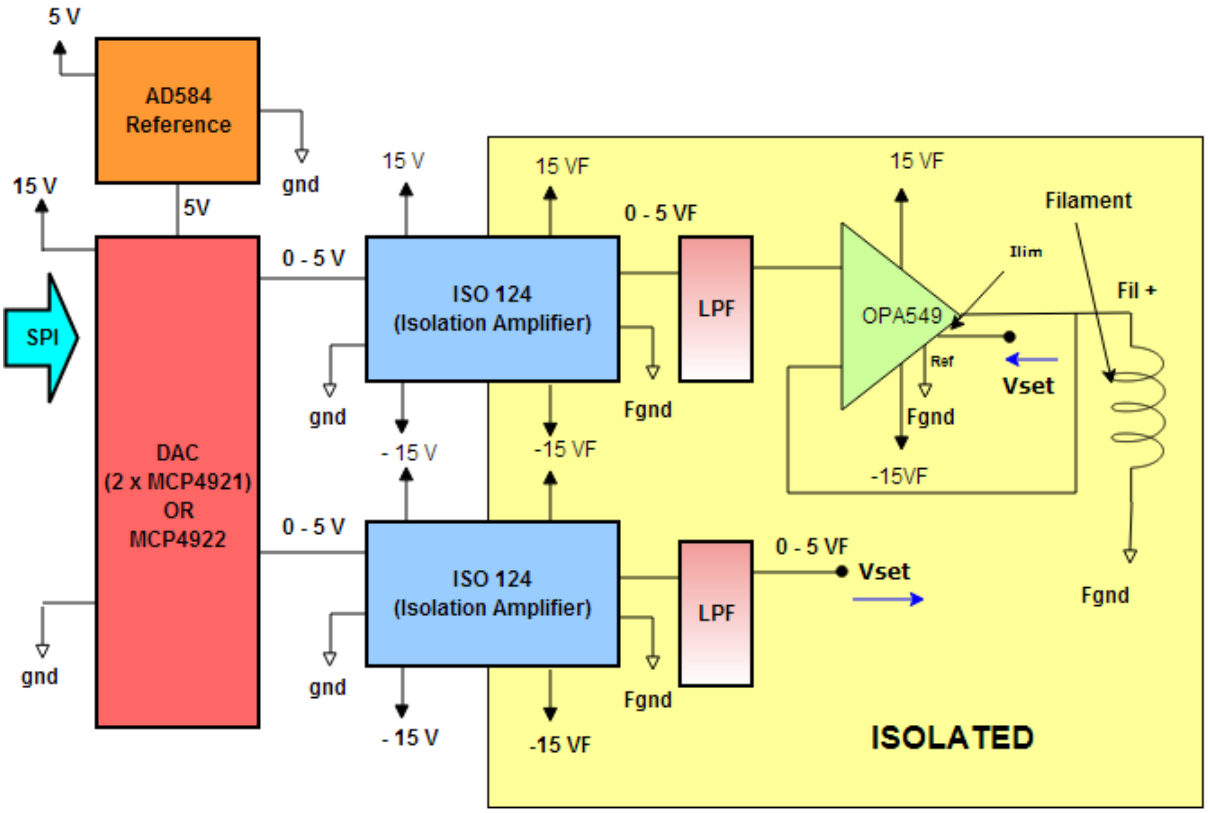

Figure 3.11: Digital control of the OPA549 output current limit

The output current limit I_{LIM} can be adjusted by varying the DAC output voltage V_{SET} according to the following equation [22]:

$$V_{SET} = (Ref) + 4.75V - (7500\Omega)(I_{LIM})/15800 \tag{3.4}$$

In equation 3.4, Ref is the floating ground potential (fgnd) in the filament driver boards.

By setting an upper limit to the current through the filament, the filament can be protected against accidental overheating. V_{SET} can be specified by the embedded controller software based on the type of filament used, thereby providing a protection mechanism for all kinds of filaments.

3.3.7 Disabling the filament current

Figure 3.12 illustrates the implementation of a function to disable the filament driver circuit.

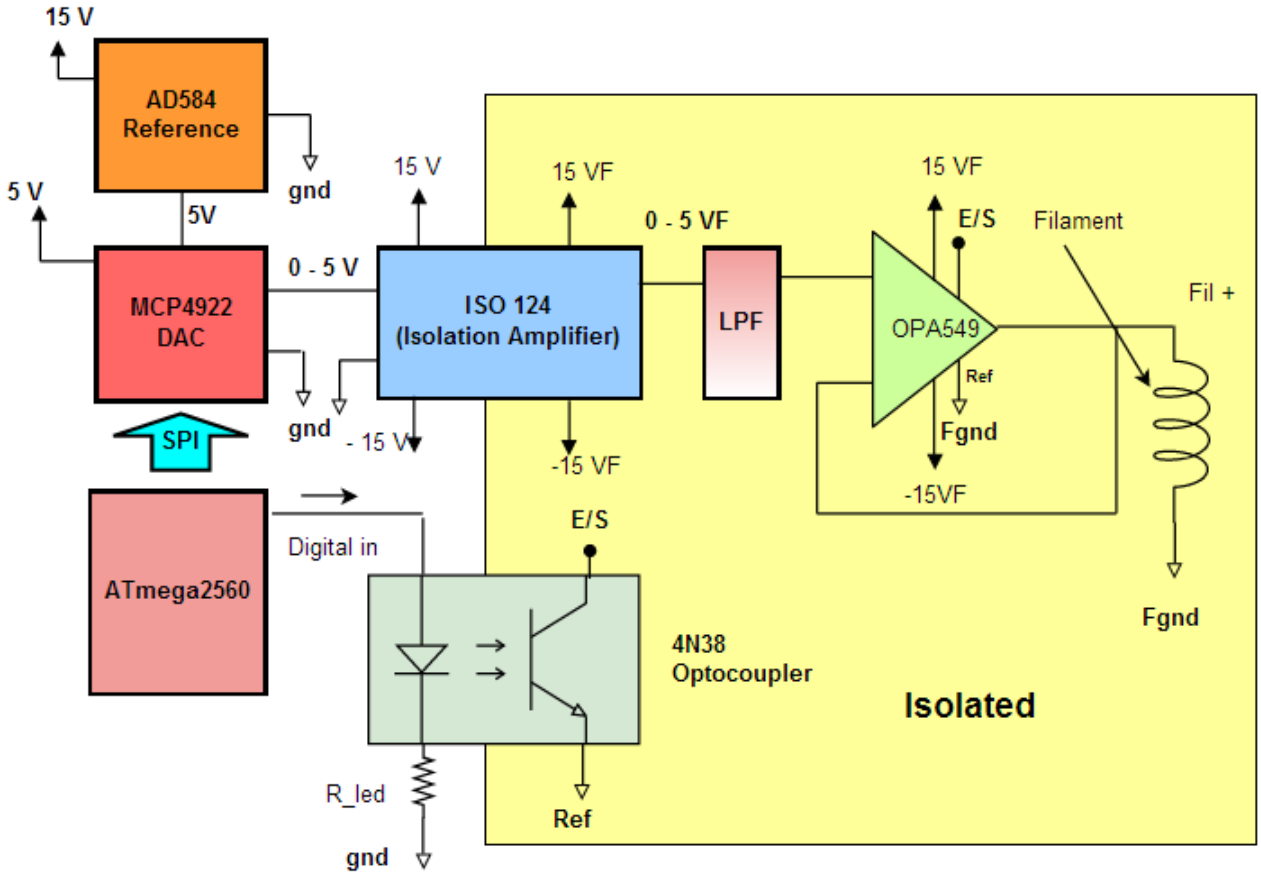

Figure 3.12: Filament current disabling with the E/S pin

Although the current through the filament can be turned off from the DAC, it is desirable to have this function at the last stage of the control electronics - the power amplifier.This late stage shutdown mode is necessery because even when the control signal is nulled by the DAC, the supply voltages on the operational amplifier might cause it to have a small output that can induce unwanted current through the filament. Therefore the E/S (Enable/Status) pin on the OPA549 is used to disable the output of the amplifier, thus shutting off the electron emission. To disable the amplifier output, the E/S pin needs to be pulled down to a logic

low (no greater than 0.8V above the Ref). An opto-isolator (4N38) rated for an isolation voltage of 5000 V_{rms} is used to isolate the microcontroller and the filament electronics. The 50 Ω resistor referred to as R_{LED} is connected in series with the opto-isolator LED. When the optocoupler is turned on by a signal from the microcontroller, it pulls the E/S pin to logic low(fgnd), disabling the output.

3.3.8 Monitoring thermal shutdown

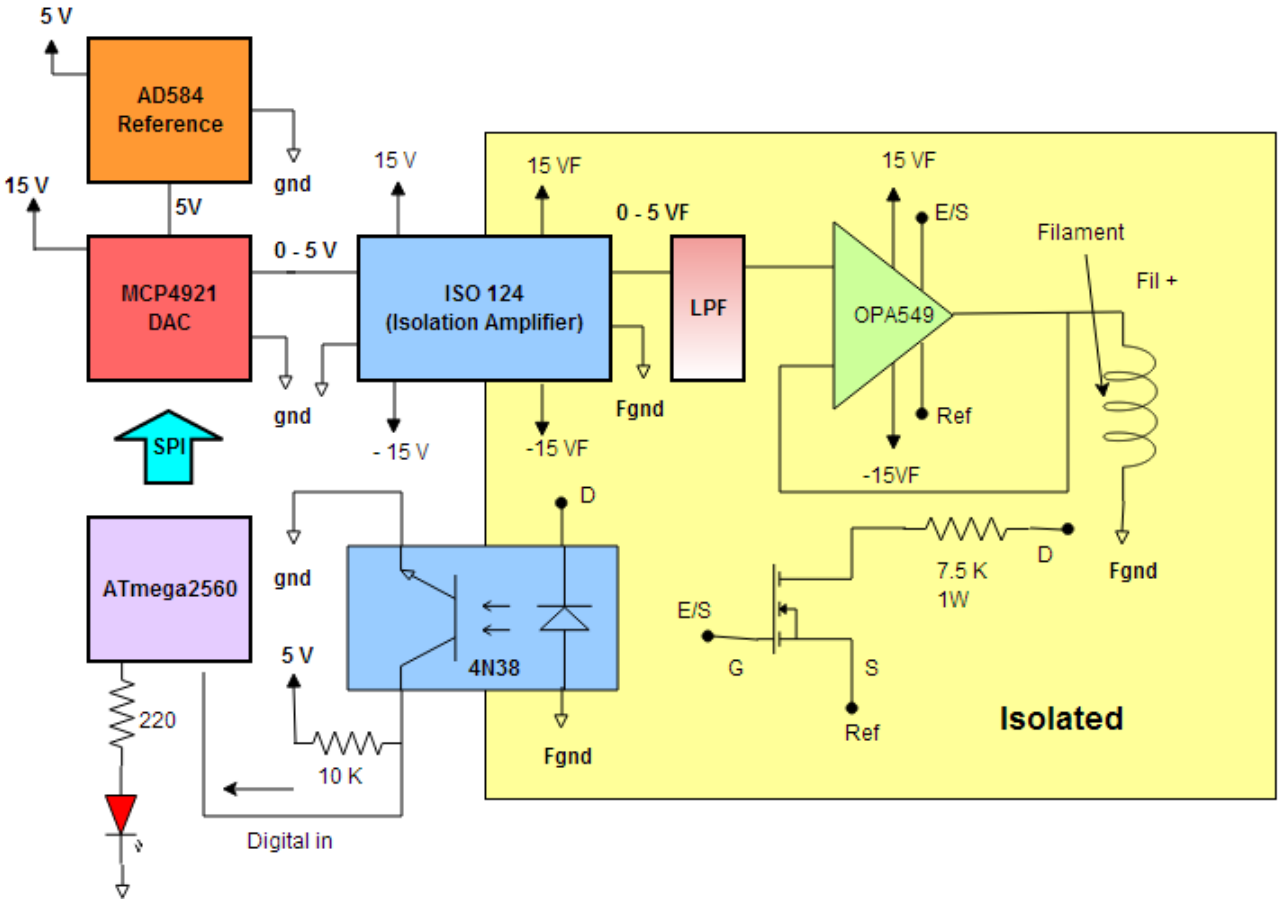

Figure 3.13: Monitoring the thermal shutdown with the E/S pin

Due to the high current output of the power amplifier the chip is prone to overheating. The intrinsic thermal shutdown circuitry of the OPA549 protects it from damage. It might be useful to display when the output is disabled due to overheating of the filament driving amplifier. The thermal shutdown circuitry disables the output when the junction temperature reaches 160 °C . Once the temperature cools down to 140 °C the output is automatically enabled. Depending on the load conditions, the thermal protection circuitry might cycle on and off . The same E/S pin on the amplifier can be monitored to determine if the device is shut down due to overheating. Normally, the E/S pin is about 3.5V above the reference

(in this case, Fgnd). If the device is shut down, the voltage on the E/S pin drops to 200mV above the Ref.

The implementation of this circuit is shown in Figure 3.13. Again, the optocoupler 4N38 is used to isolate the filament and the controller side. On the filament side, an N channel MOSFET - ZVN3310 is introduced. The E/S pin is connected to the gate of the MOSFET and as long as the amplifier functions normally, the IR-LED inside the coupler is on and the microcontroller gets no signal. When the E/S pin voltage drops due to the thermal protection circuit, the optocoupler is turned off and the digital input pin to the microcontroller is pulled up to logic high (5V). The microntroller can use this information to warn a user about thermal shutdown with a blinking LED.

3.3.9 Heat sinking of the Power amplifier

To ensure reliable operation of the OPA549 power amplifier it needs to be heat sinked properly. The junction temperature in the power amplifier package rises due to the power dissipated by the amplifier. In this section, the selection of a heat sink is discussed based on the power dissipated by the amplifier. The junction temperature T_J can be determined according to the equation:

$$T_J = T_A + P_D(\theta_{JC} + \theta_{CH} + \theta_{HA}) \tag{3.5}$$

where,

- T_J is junction temperature
- T_A is ambient temperature
- P_D is power dissipated
- θ_{JC} = junction-to-case thermal resistance
- θ_{CH} = case-to-heat sink thermal resistance
- θ_{HA} = heat sink-to-ambient thermal resistance
- θ_{JA} = junction-to-air thermal resistance

Assuming the maximum current through the filament is 3A, the power P_D dissipated by the power amplifier can be calculated by:

$$P_D = I_L(V_S - V_O) = 3A(9v - 3v) = 18W \tag{3.6}$$

V_S and V_O in the equation are the supply and the output voltages respectively. The 11 lead T-220 power package OPA549 has $\theta_{JC} = 1.4\,^{\circ}\mathrm{C}/W$ according to the specification table

in the OPA549 datasheet. The typical θ_{CH} for a mounted 11-pin power T-220 package is $0.5\,^{\circ}\mathrm{C}/W$. Based on this information, assuming a maximum ambient temperature of $40\,^{\circ}\mathrm{C}$ and using equation 3.5, the heat sink-to-ambient thermal resistance can be solved to satify the constraint that the junction temperature needs to be kept below $125\,^{\circ}\mathrm{C}$. This will provide a safety margin of ($160\,^{\circ}\mathrm{C}$ - $125\,^{\circ}\mathrm{C} = 35\,^{\circ}\mathrm{C}$).

Solving Equation 3.5 for θ_{HA}:

$$\theta_{HA} = (T_J - T_A)/P_D - \theta_{JC} - \theta_{CH} = 2.82\,^{\circ}\mathrm{C}/W. \tag{3.7}$$

Therefore, for the junction temperature to stay below $125\,^{\circ}\mathrm{C}$, the heat sink selected must have a θ_{HA} below $2.82\,^{\circ}\mathrm{C}/W$.Since the power dissipated is 18 W (Equation 3.6), for the junction temperature to stay below $125\,^{\circ}\mathrm{C}$, the sink temperature must stay below $2.82\,^{\circ}\mathrm{C}/W \times 18W = 50.76\,^{\circ}\mathrm{C}$. Armed with this information, the heat sink selected for the package was Thermalloy 6400B-P2G with thermal resistance θ_{HA} of $2.70\,^{\circ}\mathrm{C}/W$. At 18 W the heatsink temperature rises to $2.70\,^{\circ}\mathrm{C}/W \times 18W = 48.6\,^{\circ}\mathrm{C}$ which is within the chosen safety margin.

3.3.10 The full filament driver board

In summary, the filament driver board has:

1. A power amplifier for driving the filament;
2. Precision resistors for sensing the emission and the filament currents with the supporting electronics to buffer and feed that data to the ATmega2560 ADC;
3. Isolation amplifiers to isolate the filament and the microcontroller electronics;
4. Low pass filters to attenuate the high frequency noise on all isolation amplifier outputs;
5. A circuit for monitoring the applied voltage across the filament to provide data on the changing resistance of the filament;

Although left out in the simplified schematics, in both voltage control boards and filament driver boards the power pins have bypass capacitors of 0.1 μF (ceramic) to the ground and an additional 10 μF capacitor (tantalum) in parallel to attenuate high-frequency feed-through noise in the circuit. The schematics for the entire filament board are presented in Appendix B.

The following elements were not included in the first iteration of IonSim electronics, but will be incorporated into the final product.

1. Digital control of output current limit to protect filaments from overheating;
2. Optocouplers (4938s) and N channel CMOS to monitor the E/S pins for thermal shutdown
3. A circuit for driving the E/S pin to logic low for disabling the current output of the power amplifier.

These circuits were tested or simulated independently, but were not included in breadboard or PCB circuits that were used to take the data presented later in this thesis.

3.4 Dedicated Microcontroller

3.4.1 The SPI-DAC interface

As mentioned before, the dedicated microcontroller (ATmega2560) is used to control five voltage regulator boards and four filament driver boards via a SPI interface with the DACs on each of these boards (Figure 3.1). The controller, therefore, acts as a master to 9 12-bit DACs (slaves).

The SPI bus consists of four logic signals:

- SCLK - serial clock.
- MOSI - master output slave input.
- MISO - master input slave output.
- SS - Slave Select.

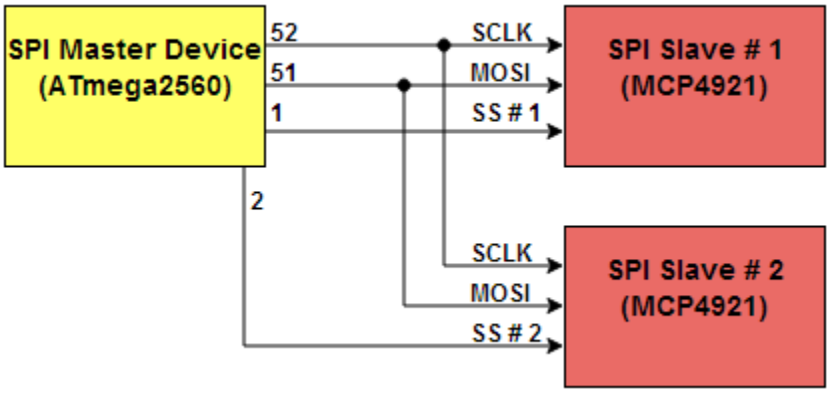

Figure 3.14: Single Master and multiple slaves with SPI bus

For the purposes of IonSim, only three of these signals are used. The DACs provide no feedback to the microcontroller, and therefore, there is no MISO in the SPI bus. The slave

devices (MCP4921s) share the SCLK and the MOSI lines - however each slave needs to have its own SS line. The arduino SPI library is used in this embedded software. Therefore, by default, the digital I/O pin 51 acts as MOSI, and pin 52 acts as SCLK in the microcontroller. Figure 3.14 illustrates multiple MCP4921 connections to the microcontroller. The SPI interface to only two out of nine DACs is shown in this illustration.

3.4.2 Digital I/O and Analog inputs to the microcontroller

All four filament driver boards provide two essential analog feedbacks signals - the filament current and the emission current. The voltage boards provide five analog voltage readings as well. Therefore, a total of 13 out of 16 available analog inputs are used, leaving a small margin. There are not enough analog inputs available to measure the voltage difference across all four filaments in order to compute the changing resistance of the filaments. Therefore, an 8-Channel analog multiplexer/demultiplexer is used to expand the analog inputs to the ATmega2560. A 74HC4051 multiplexer gives a total of eight analog inputs at the cost of 3 digital outputs and one analog input.The expansion circuit is shown in Figure 3.15.

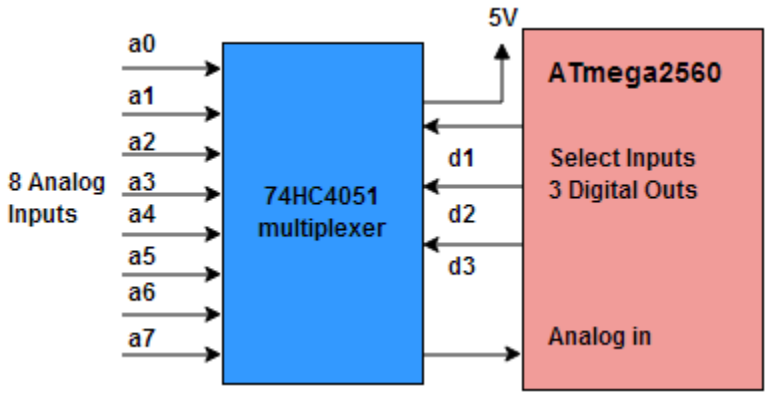

Figure 3.15: Expansion of Analog Inputs with a 4051 multiplexer

To select the analog pin that needs to be read, the three digital outputs (d1, d2 and d3) of the microcontroller are used. Each of these pins is associated with a number (d1 = 1, d2 = 2, d3 =4). These pins are toggled between logic HIGH and LOW to select an analog channel.

For example :

- If d1 and d2 are HIGH, and d3 is LOW, analog channel a3 is selected. (1+2 =3)
- If d2 and d3 are HIGH and d1 is LOW analog channel a6 is selected (2+4 =6)

- if d1, d2 and d3 are LOW, analog channel a0 is selected.

The selected analog channel is read by the microcontroller from the sole "Analog in" between the multiplexer and the ATmega2560.

The ATmega2560 microcontroller has 54 digitial I/O pins and 16 analog input pins. With 9 slave devices (DACs) only 11 digital I/O pins are used for SPI interface. Moreover, 2 digital outputs for each filament (a total of eight for 4 filaments) are used to display overheating and filament replacement status with blinking LEDs. Three more digital I/O pins are used for expanding the analog inputs. Therefore, only 22 out of 54 available digital I/O pins are used. With the multiplexer, the controller has 23 analog inputs, out of which only 17 are used. This leaves margin for future expansions for both digital and analog pins.

It must be noted that only one out of four filaments were used for taking data and therefore the multiplexer was not needed in the circuit that took data for this thesis.

Chapter 4

Software Control for ion Source

4.1 Overall Software Architecture

As mentioned in section 3.1, a PC running LabView is connected to an ATmega microcontroller via USB. The microcontroller receives serial commands from a Labview interface and controls the voltages on the ion source surfaces and the filament emission. Real time analog feedback on the status of the emission is received by the microcontroller. These data are used in keeping the emission stable. A flowchart of the entire process is shown in Figure 4.1.

Based on the user input to the LabView interface, a serial data array of the format (a,b,c,d,e,f) is generated by LabView and sent to the ATmega processor via serial communication over USB. If the serial command sent from the LabView UI (user interface) contains incompatible data, an error is shown in the error display field of the UI. The data are then parsed, and based on the parameters a, b, c, d and e the voltage biases for the repeller, chamber, grid, ring and the filaments are set. Since a 12 bit DAC is used to set the voltage biases, these parameter values range from 0 - 4095 which corresponds to a 0 to $\pm$ 200V bias. All four filaments are set to the same voltage bias. The voltage biases are set before the filament currents are set and stabilized.

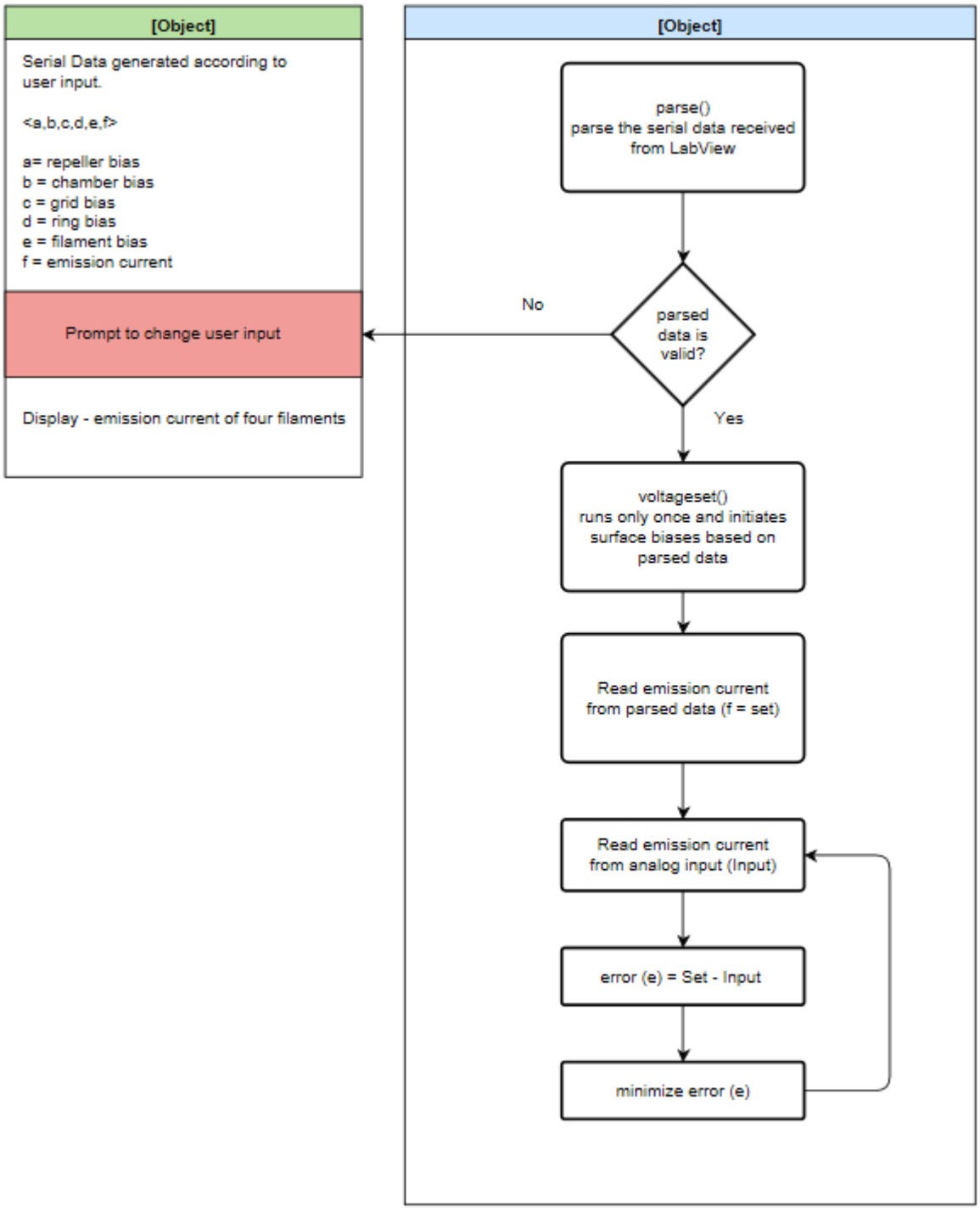

Figure 4.1: Overall software architecture

Once the voltages are set, the filament emission is controlled based on the f parameter of the

parsed serial data. All four filaments are set to emit the same emission current. To keep the filament emission constant, the electron emission from each filament is measured and fed into an analog input to the microcontroller. This information is then compared to the f parameter and an error is calculated. Unlike setting the voltage biases, this process is continuously repeated in a loop so that the error is continuously minimized. The procedure for setting the voltage biases and the mechanics for keeping the electron emission constant on all four filaments are discussed later in this chapter. The analog input pins that receive the emission data and the output pins that control the DACs are hardcoded in the microcontroller program and cannot be changed from the LabView UI .

4.2 LabView User Interface

A preliminary LabView UI that sends the serial data to the microcontroller program is shown in the figure below:

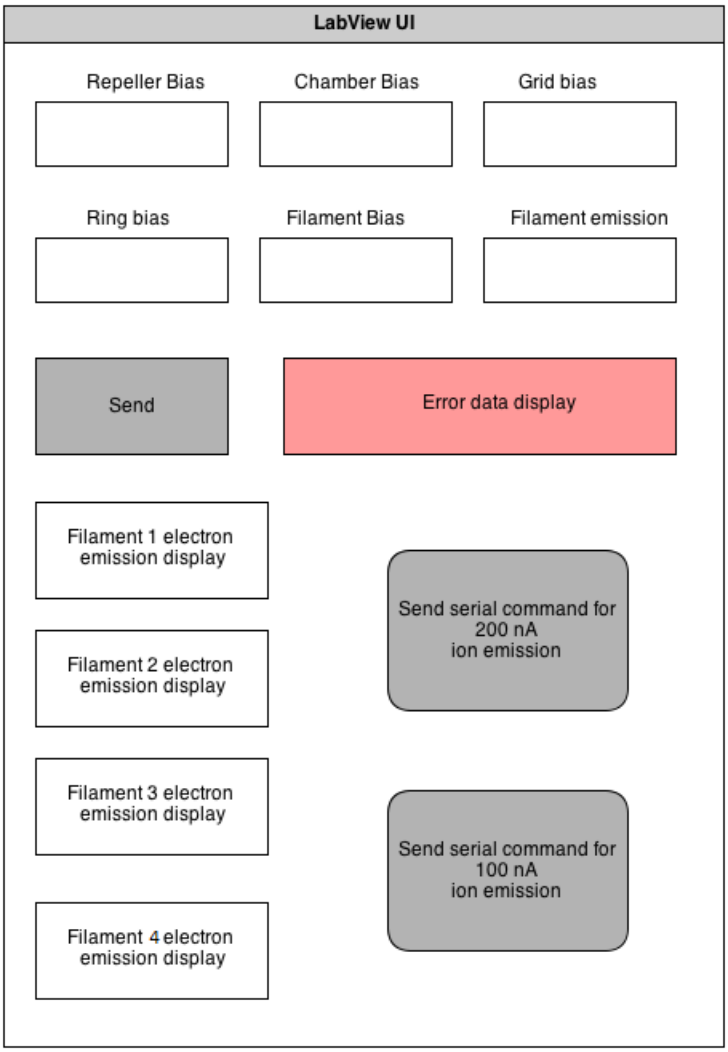

Figure 4.2: Labview UI

The electron emission currents from the filaments, as read by the analog input pins of the microcontroller are shown in four electron emission display fields in the user interface, as shown in Figure 4.2. The incoming 0-1023 serial data gathered by the 10 bit ATmega ADC

analog inputs is changed to meaningful units (μA) before being displayed.

Moreover, based on experimental data, two preset serial data packages can be sent to the microcontroller program for two specific ion emission currents (represented by 100nA and 200nA in the figure). The serial data arrays of the format (a,b,c,d,e,f) to obtain these ion emissions are hardcoded in the LabView program and are specific to the filaments used in the ion source.

4.3 Microcontroller Program

4.3.1 Setting Voltage Bias

To set the voltage bias on different surfaces, first the serial data from LabView are parsed by the ATmega microcontroller. The program statements to parse the incoming serial data are shown in the Listing 4.1 below:

Listing 4.1: Parsing.

```
const int NUMBER_OF_FIELDS = 6;
int fieldIndex = 0;
int values[NUMBER_OF_FIELDS];

 if (Serial.available())
   {
     char ch = Serial.read();
     if(ch >= '0' && ch <= '9')
     {
       if(fieldIndex < NUMBER_OF_FIELDS)
         {
            values[fieldIndex] = (values[fieldIndex] * 10) + (ch - '0');
         }
     }
     else if (ch == ',')
     {
       fieldIndex++; // increment field index
     }
     else
     {
```

```
        repeller = values[0];
        chamber = values[1];
        grid = values[2];
        ring = values[3];
        filament = values[4];
        emission = values[5];
    }
```

The number of fields to be parsed is set in line 1 and the first five elements in the values [ ] array are used to set the voltage biases on the ion source surfaces. Then, based on the parsed values and the hardcoded output pins , the voltages are set using the 'set( )' function as shown in Listing 4.2. The microcontroller is connected to the DACs that set the voltage biases with a Serial Peripheral Interface (SPI) bus. The SPI library of the Arduino is used for convenience as shown in Listing 4.2.

Listing 4.2: set () function .

```
#include "SPI.h"

word outputValue = 0;
byte data = 0;

// voltage control pins
pinMode(10, OUTPUT); //repeller
pinMode(2, OUTPUT); // chamber
pinMode(3, OUTPUT); // filament
pinMode(4, OUTPUT);  // focus ring
pinMode(5, OUTPUT);  // grid

void loop {
```

```
  set (10,repeller);
}
  void set(int pin, int value)
    {
        outputValue = value;
        digitalWrite(pin, LOW);
        data = highByte(outputValue);
        data = 0b00001111 & data;
        data = 0b00110000 | data;
        SPI.transfer(data);
        data = lowByte(outputValue);
        SPI.transfer(data);
        digitalWrite(pin, HIGH);
    }
```

In the example above, the set() function is used in the void loop () section of the microcontroller program to regulate the voltage bias on the repeller surface. The SPI library we are using only supports master mode, i.e, using this library the microcontroller can be only used as a master and any pin can be used as the Slave Select (SS) pin. This is adequate for our purposes. The SS pins for the SPI interface - the pins that the master (microntroller) uses to enable and disable specific slaves (DACs) are hardcoded in the microcontroller program and are set as OUTPUT between lines 34-38. The default SCK (Serial Clock) and the MOSI (Master In Slave Out) pins of the ATMega based Arduino board are shared by all the DACs. All SPI devices have a maximum allowed speed for the SPI Bus. The MCP4921 DACs support up to 20MHz. The default clock speed of the SPI library is only 4MHz and is not changed. If necessary, the clock speed can be easily changed using the library's SPI.setClockDivider() function.

The data written to the DACs were prepared based on the write command register of the DAC (MCP4921) used in the electronics. The command register is shown in Figure 4.3. Bits 0 to 11 are the 12 bits of the output value; bit 15 is an output selector (unused on the MPC4921, and is set 0 or 1 to select between the two outputs on the MCP4922); bit 14 controls the input buffer; bit 13 controls an inbuilt output amplifier; and bit 12 can shut down the DAC. The input data are spread across two bytes (or one word of data). First, a variable - outputValue (a 16-bit unsigned variable) is declared in line 30 for sending a word of data to the DAC. We can only pass one byte of data at a time through the SPI bus, so the function highbyte() is used to separate the high side of the word (bits 15 to 8) into a byte variable called data in line 47 of the set () function.

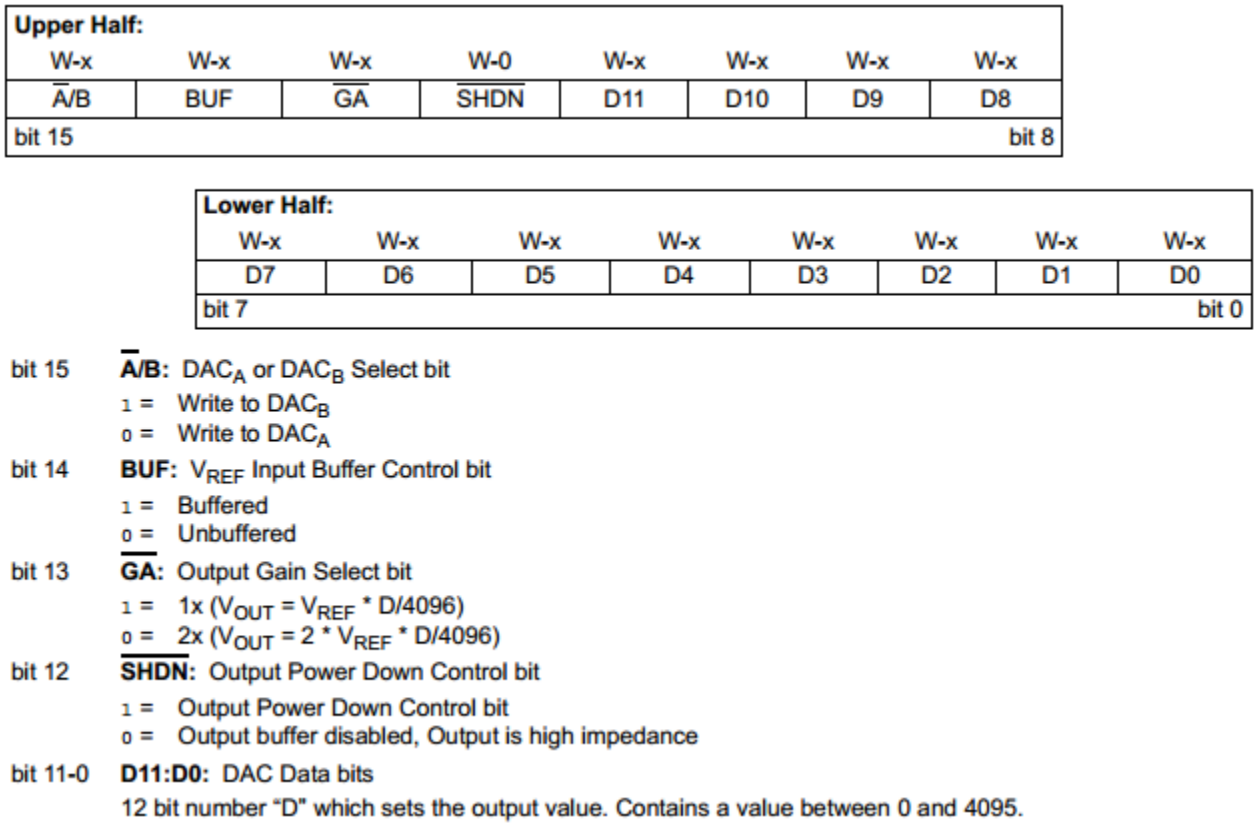

Figure 4.3: Command registers for MCP4921/MCP4922 as seen in the chip datasheet [1].

Next, the bitwise AND and OR operations are used in lines 48 and 49 to set the parameter bits 15 -12. The byte is then sent using the SPI library's SPI.transfer( ) function in line 50. Finally, the lowbyte ( ) function is used to separate and send the rest of the word.

Due to the sporadic performance issues noticed during testing, all voltage controlling DACs are calibrated to 0 V output before a voltage bias is set using the simple calibration function shown in the Listing 4.3 below:

Listing 4.3: calibration () function .

```
void calibration (int pin) {
    for (int i = 0; i < 5; i++) {
      outputValue = 0;
      digitalWrite(pin, LOW);
      data = highByte(outputValue);
      data = 0b00001111 & data;
      data = 0b00110000 | data;
      SPI.transfer(data);
      data = lowByte(outputValue);
      SPI.transfer(data);
      digitalWrite(pin, HIGH);
      delay(1000);
    }
```

4.3.2 Filament Emission Control - A simple one bit integrator control

Parsed data from the LabView serial command are used for emission control. The sixth value of the values [ ] array (Listing 4.1) is used to set the electron emission on all four filaments. The same DACs (MCP4921s/22s) are used to control the filament currents that produce the required electron emissions, and these are similarly controlled over the SPI bus. The code used to control the electron emission, therefore, is very similar to the listings already discussed. A simple feedback controller that increased or decreases the DAC output by one bit is used to keep the filament emission stable. The controller ( ) function used to keep the emission stable is shown below in Listing 4.4:

Listing 4.4: calibration () function .

```
  // filament control channels
  int fila = 5;
  int filb = 6;
  int filc = 7;
  int fild = 8;

  // filament inputs
  int valuea = 1;
  int valueb = 2;
  int valuec = 3;
  int valued = 4;

 // filament current limit
  int limit = 3000;

void setup()
```

```
  {
      //filament control pins
      pinMode(5, OUTPUT);
      pinMode(6, OUTPUT);
      pinMode(7, OUTPUT);
      pinMode(8, OUTPUT);

      SPI.begin();
      SPI.setBitOrder(MSBFIRST);
      Serial.begin(9600);
    }
void loop() {
            control = value [5];
              // filament 1
               controller(fila, valuea, control);
              // filament 2
               controller(filb, valueb, control);
              // filament 3
               controller(filc, valuec, control);
              // filament 4
               controller(fild, valued, control);
}

void controller(int controlpin, int inputpin, int control)
    {
        input = 0;
        for (int i = 0; i < 5; i++) {
          input = input + analogRead(inputpin);
```

```
      delay(time);
    }// end for loop
    input = input/5; // moving average

if (input < control) outputValue = outputValue+1;
if (input > control) outputValue = outputValue-1;

if (outputValue < limit)
  {
      digitalWrite(controlpin, LOW);
      data = highByte(outputValue);
      data = 0b00001111 & data;
      data = 0b00110000 | data;
      SPI.transfer(data);
      data = lowByte(outputValue);
      SPI.transfer(data);
      digitalWrite(controlpin, HIGH);
  }
 else {
      digitalWrite(controlpin, LOW);
      data = highByte(limit);
      data = 0b00001111 & data;
      data = 0b00110000 | data;
      SPI.transfer(data);
      data = lowByte(limit);
      SPI.transfer(data);
      digitalWrite(controlpin, HIGH);
 }
```

}

The analog input pins that read the filament emission current and the Slave Select (SS) output pins for controlling the DACs are hardcoded in lines 70 -80. Then the controller () function is used in the void loop () to control all four filaments.

The controller () function implements the following steps:

1. The specified emission current is read from the predefined analog input.
2. A moving average is performed on these inputs to cancel out the noise (lines 111 - 116).
3. The hysteresis control is performed in lines 117-118 by comparing the input to the desired output.
4. The output is only applied if it is less than a predefined limit.

There was a noticeable increase in performance when the moving average was applied to reduce noise. Based on the filtered input, the controller makes the smallest changes permitted by the 12 bit DAC . Since the voltage that controls the filament current is between 0 - 5 V, the smallest changeable voltage with the 12-bit DAC is $\frac{5}{4096}$ Volts or 1.22 mV.

During testing it was observed that the filaments break if the current through them is more than 1.2 Amperes. For this reason a limit was introduced. The upper limit (3000 corresponding to 3.66 V) of the voltage applied across the filament is hardcoded in the program in line 82 (Listing 4.4). Under no circumstance is this limit exceeded while controlling the emission current. This limit will vary with the type of filament used. Moreover, the resistance of the filament changes as it heats up. Therefore it is not easy to calculate this limit theoretically; it is best determined experimentally. For the filaments in use during data collection for this project, the 3.3 V limit is appropriate. The entire embedded software for voltage boards and the filament drivers is listed in Appendix C.

4.3.3 Proportional-Integral-Derivative (PID) controller

Along with the simple hysteresis controller, a PID controller to stabilize the electron emission was also tested. A PID function runs in a loop to keep the emission stable and performs the following calculation:

$$CO = K_c \left(e(t) + \frac{1}{T_i} \int e(t)dt + T_d \frac{dPV}{dt} \right) \tag{4.1}$$

where

- CO is the controller output, in our case the control input sent to the DACs (0-4095)
- K_c is a proportional tuning constant
- e(t) is the error at time t
- T_i s an integral tuning constant
- T_d is a derivative tuning constant
- dt is the rate the loop runs at
- PV is the process variable, in our case the electron emission as seen by the 10-bit ADC on the analog input pins of the microcontroller (0-1023).

The PID controller for our application was tuned by fitting a simple first order plus dead time (FOPDT) dynamic model to emission test data. The FOPDT dynamic model has the form:

$$T_p \frac{dPV}{dt} + PV(t) = K_p.CO(t - \theta_p) \tag{4.2}$$

where,

- PV(t) = measured process variable as a function of time
- CO(t θ_p) = controller output signal as a function of time and shifted by θ_p
- θ_p = process dead time
- t = time.

At first, the change of process variable with respect to controller output was recorded using a step test. The input to the DAC (CO) was simply "stepped up" to a new value and the analog input to the ADC caused by the electron emission (PV) was observed. These data were then used to find the parameters T_p, K_p and θ_p. Both analytical curve fitting and simple graphical methods can be used to find these parameters. Once the dynamic model parameters are found, PID tuning parameters (K_c, T_i and T_d) can be found from the dynamic model parameters (T_p, K_p and θ_p) using well defined relations in the literature [25], and various controls can be tested out.

For example, in a moderate P-only controller : $K_c = \frac{0.2}{K_p}\left(\frac{T_p}{\theta p}\right)^{1.22}$ and in a PI controller: $K_c = \frac{1}{K_p}\left(\frac{T_p}{\theta p+T_p}\right)$ and $T_i = T_p$.

Figure 4.4 below shows the results of a PID controller with optimized proportional and derivative tuning parameters. Although PID was successful in stabilizing the electron emission, a simpler one bit integrator control was chosen over a PID controller because:

1. There were no improvements in the output variance with a PID controller. Both hysteresis and PID controller achieved in keeping the variance less than 1%.
2. The tuning parameters need to be changed every time filament characteristics change to keep the variance less than 1%.
3. Although the settling time improved with a PID controller, setlling time with the simpler controller was adequate for this application.

4. Minor overshoot was observed wth optimized parameters. This overshoot can eliminated with further tuning, but it may reappear if the filament characteristics change.

5. One bit integrator controller is simple compared to PID controller.

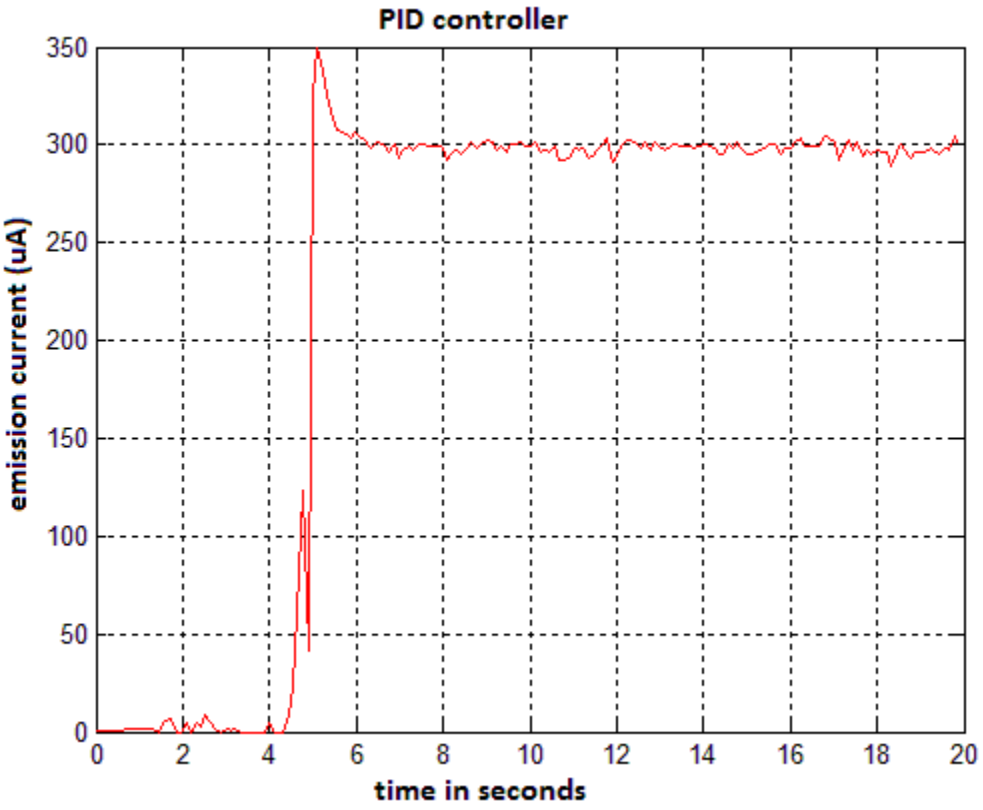

Figure 4.4: PID controller

The need for tuning the PID parameters every time the filament characteristics change is the major reason for choosing the one bit integrator controller over the PID controller. The filament emission characteristics can change when:

1. A new filament material is used;

2. A filament gets worn out with continuous use;

3. As the pressure in the vacuum chamber changes.

Figure 4.5 below shows the change of filament characteristics in an oxygen rich environment for two types of filament. The data is based on a different study done by Dr. Ryan Davidson in 2012, and clearly shows the difference in initial resistance in two differnt kinds of filaments and the change of filament resistance over time. The top plot represents the change of resistance in a Tungsten-Rhenium(W-Re) filament with a 0.1 mm diamter, while the bottom plot represents the characteristics of a Tungsten-Rhenium(W-Re) filament with rectangular dimensions of 0.05 mm by 0.09 mm.

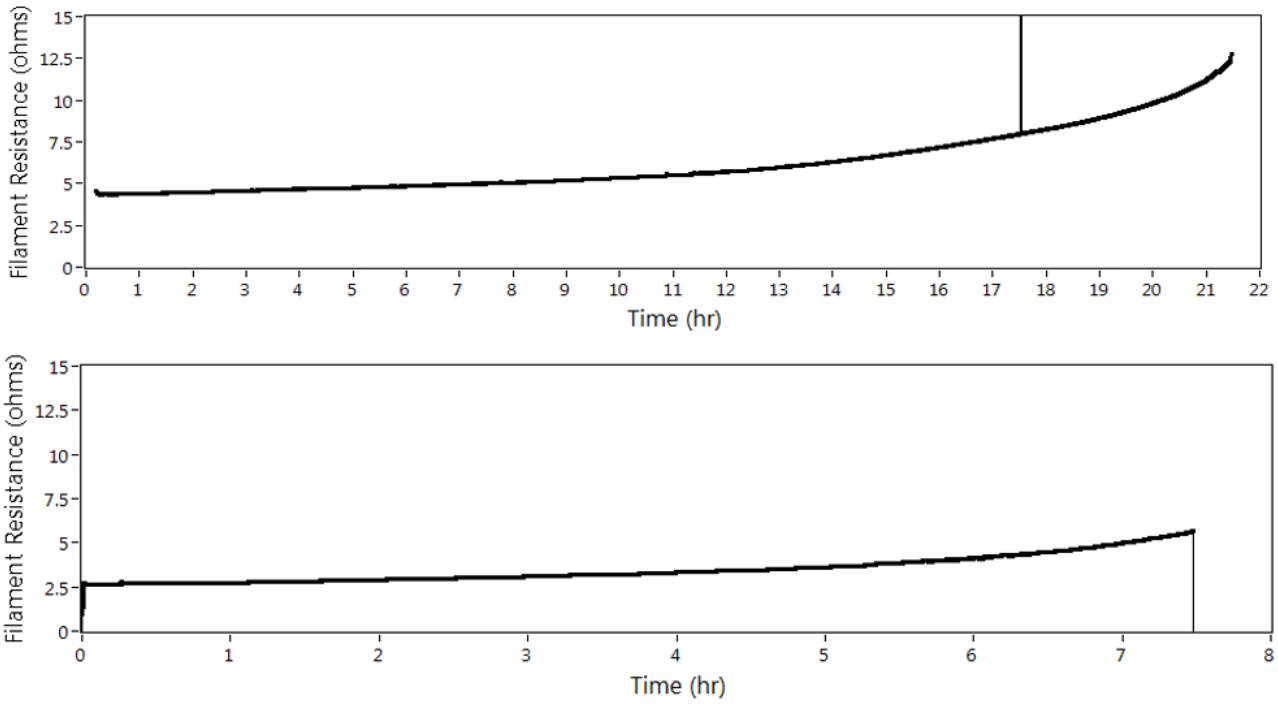

Figure 4.5: Filament resistance change over time in two different filament types. The image is used here with permission from Dr. Ryan Davidson

Moreover, the overshoot (as seen in Figure 4.4) may appear when the filament characteristics change, and this overshoot may damage the filament if the filament current surpasses the safety limit as discussed earlier in the chapter. An model reference-based adaptive PID

controller can be used in our application, but that will makes the controller for our application complex. This adaptive controller may be more efficient than the one bit integrator controller and can be a future research topic.

4.4 ATmega- Serial Interface

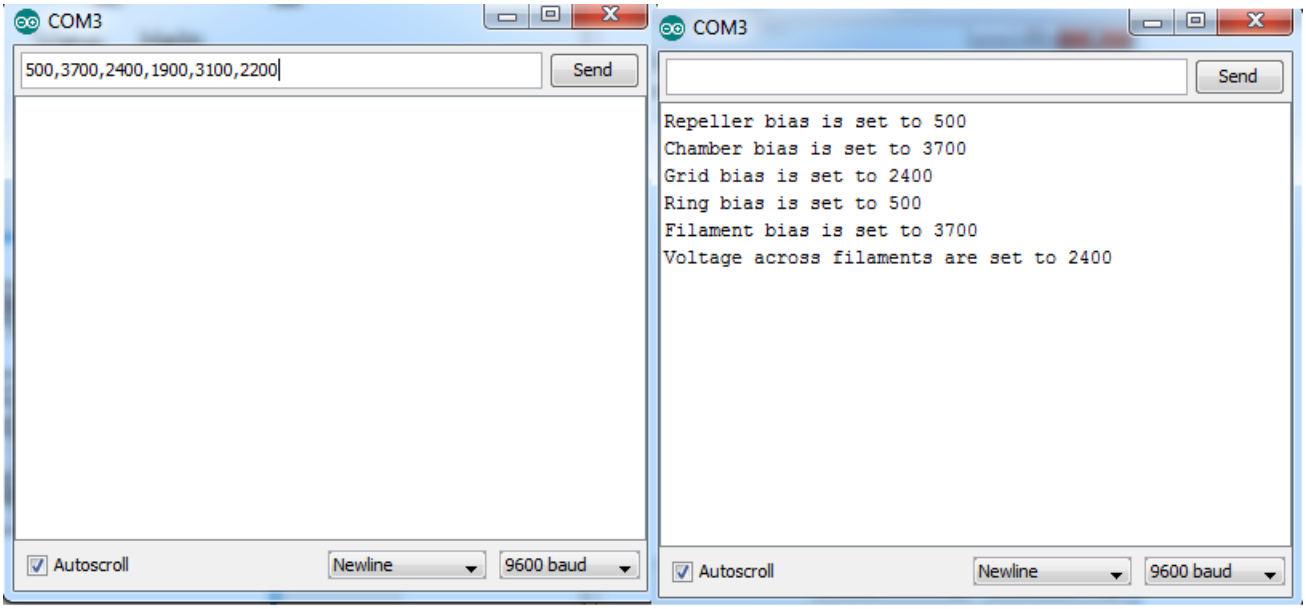

Figure 4.6: Controlling IonSim by using the simple serial monitor that comes prepackaged with Arduino IDE.

The microcontroller program is designed to accept serial data with the format (a,b,c,d,e,f) , either manually from the serial monitor or from LabView. In fact, anything that is capable of sending serial data of this format will work. A Processing or a Matlab user interface will work just as well as a LabView user interface to connect a PC with the microcontroller. Figure 4.6 below shows the setup working with the simple serial monitor that comes prepackaged with the Arduino IDE.

Chapter 5

Experiments and Results

5.1 Filament Emission control using the simple one bit integrator

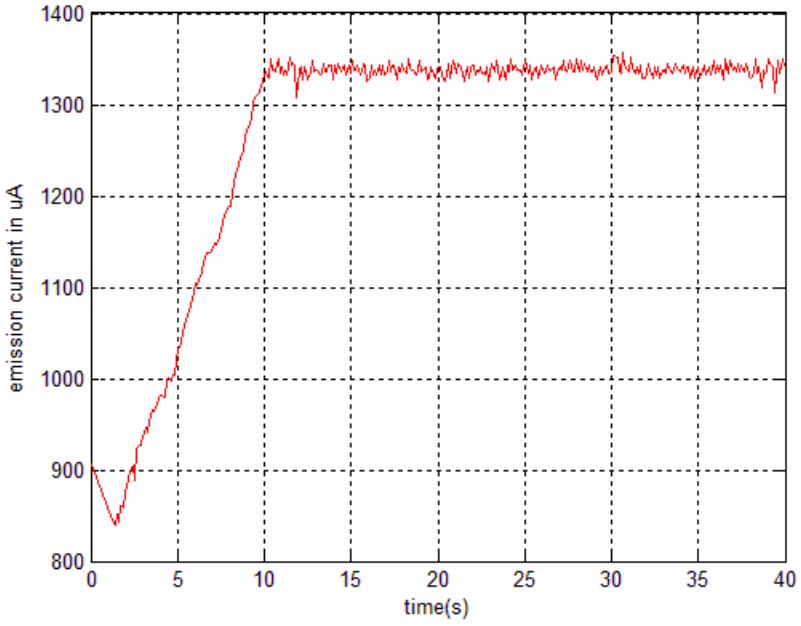

Figure 5.1: Electron emission control with a simple integrator controller

The results for the one bit integrator control on a filament are depicted in the figure 5.1. It takes about 10 seconds to reach the emission level of 1340 μA in the example, but this is acceptable in our application. This enables the small change steps shown in lines 117-118 of the listing **??** to be safely used.

Less than 1% variance of the electron emission was observed while using the integrator controller shown in Figure 5.2. This also meets the design criteria for the ion source. The blue dotted lines in Figure 5.2 represent the upper and the lower bounds of 1% variance around the electron emission for 1340 μA (The electron emission we were trying to achieve).

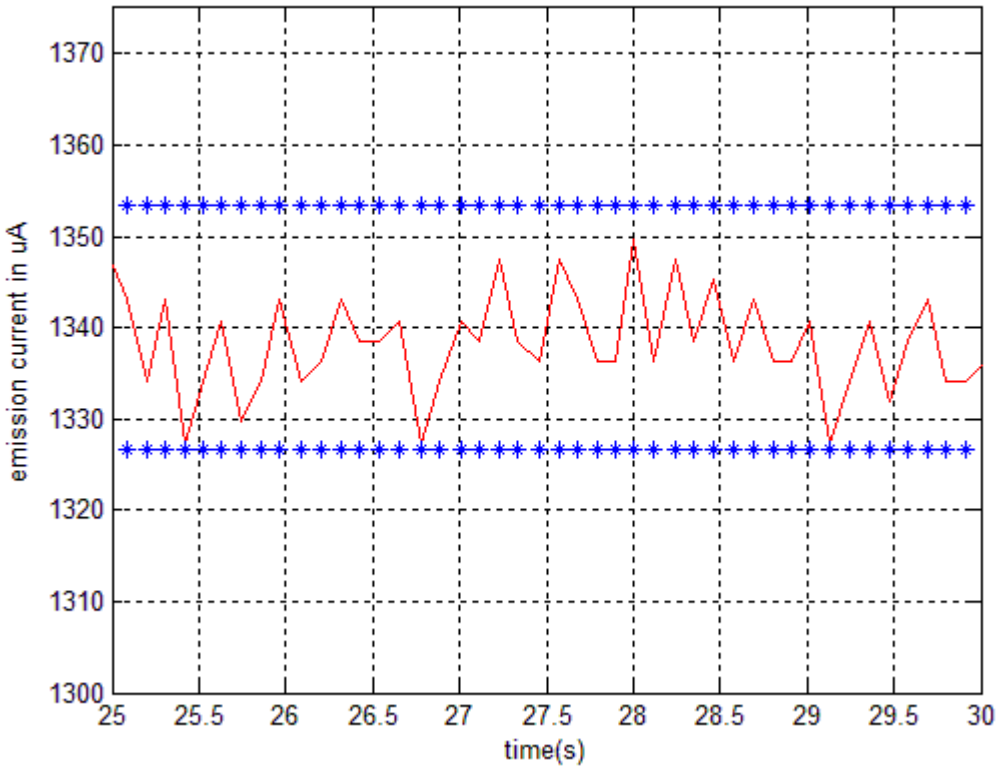

Figure 5.2: 1% variance in electron emission

5.2 Using PWM as proxy for DAC

Using the built-in analogWrite() function of the arduino language used in our microcontroller program, it is possible to use Pulse Width Modulation (PWM) to supply electrical power to a load that has a relatively slow response. Since this has the potential to make the design simpler and cheaper, this avenue was investigated. The PWM pulse train acts as a DC signal when the device that receives the signal has a response time that is significantly slower than the frequency of the pulses. The PWM pulse train in the Arduino processor operates at 500 Hz by default and the parameter that sets the duty cycle in the pulse train is an 8-bit unsigned integer , *i.e.*, it has a value in the range 0-255.

However, using pulses to heat up the filament introduces noise, and the control is implemented with higher resolution by using a 12-bit DAC instead of an 8-bit parameter that controls the PWM output. In this application the advantage of a tighter control outweighs the power issue, so the 12-bit SPI DAC was chosen over the integrated PWM output. Better results may be achieved by increasing the clock frequency driving the PWM.

5.3 Effect of surface potentials on ion emission

5.3.1 Baseline

Based on the simulation discussed in Section 2.3, the optimal biases on ion source surfaces were as follows

- Chamber bias = - 110V
- Filament = - 80 V
- Grid = - 50 V
- Focus ring = - 40 V

- Repeller = 30 V

This configuration was used as a baseline to measure the effects of changing the bias settings on the output ion current. However, despite the simulation results, no significant ion current was measured until the filament bias was lowered to around -95 V. Therefore, the baseline conditions given above were changed slightly, and the filament bias is actually -95 V.

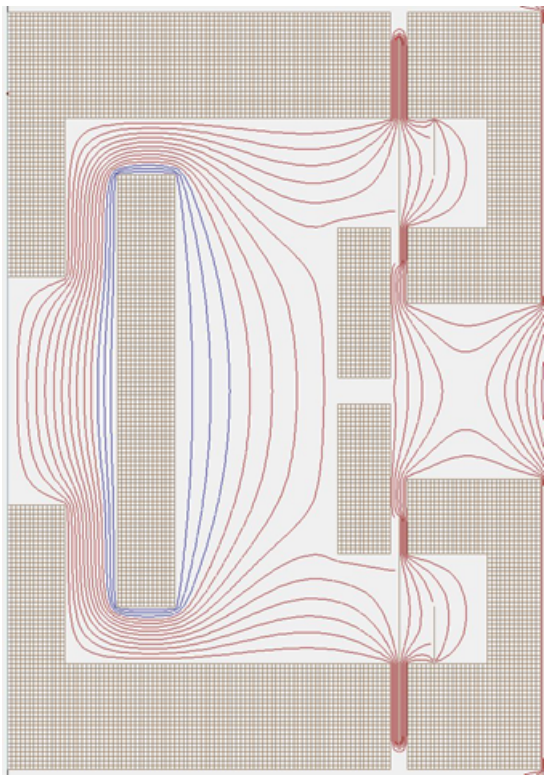

Figure 5.3: Potential map of the Ion Source generate using Simion®. This figure is reproduced with permission of Dr. Ryan Davidson

Figure 5.3 shows a potential map of the ion source based on the biases mentioned above. The equipotential lines in the map go from 20 V to -110 V. The blue lines represent the positive potentials while the red lines represent negative potentials inside the source. This map gives us an idea on how the electron and ion trajectories inside the source may look like in the absence of space charge.

5.3.2 Effect of Pressure

To make sure that the current we are measuring is truly the ion current, the pressure in the vaccum chamber that houses the ion source was varied while continuously monitoring the current. The result is shown in Figure 5.4. A linear relationship shows that the current is due to ionization of the background gas.

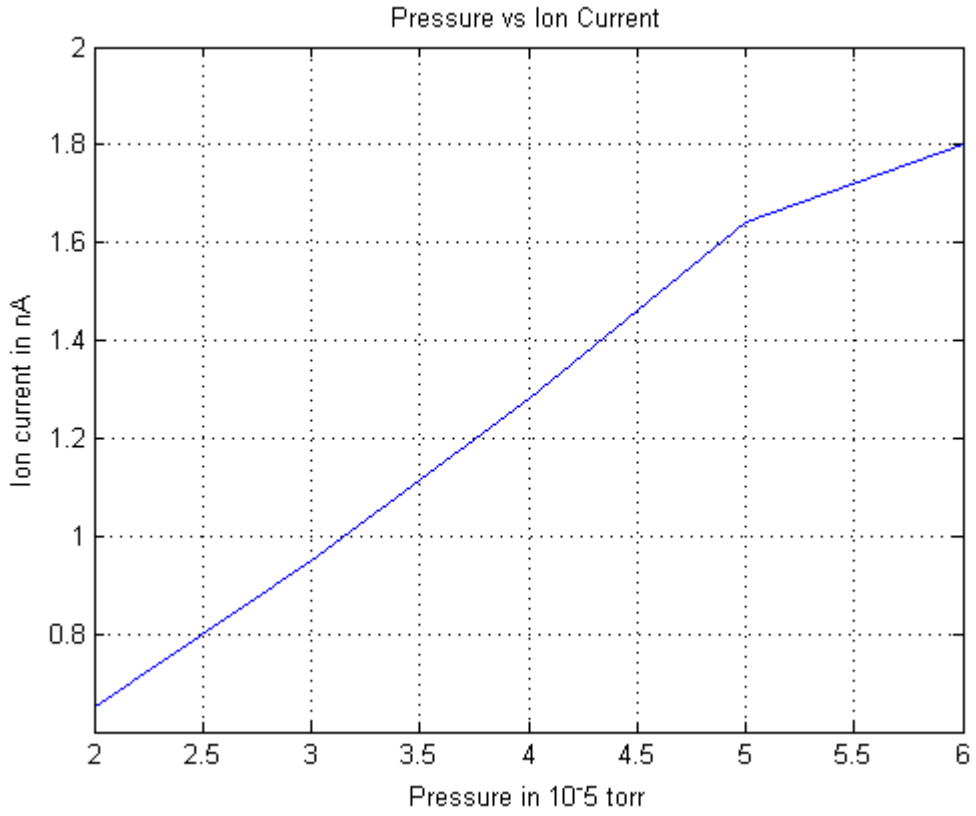

Figure 5.4: Pressure vs ion current, demonstrating the linearity expected due to ionization of the background.

The voltage biases used for this experiment were:

- Chamber bias = - 100V
- Filament = - 95 V

- Grid = - 50 V
- Focus ring = - 40 V
- Repeller = 30 V

5.3.3 Effect of Filament Bias on output ion current with emissions from a single filament

To measure the effect of filament bias on the output ion current, the filament bias was changed while keeping other biases constant at

- Chamber bias = - 100V
- Grid = - 50 V
- Focus ring = - 40 V
- Repeller = 30 V

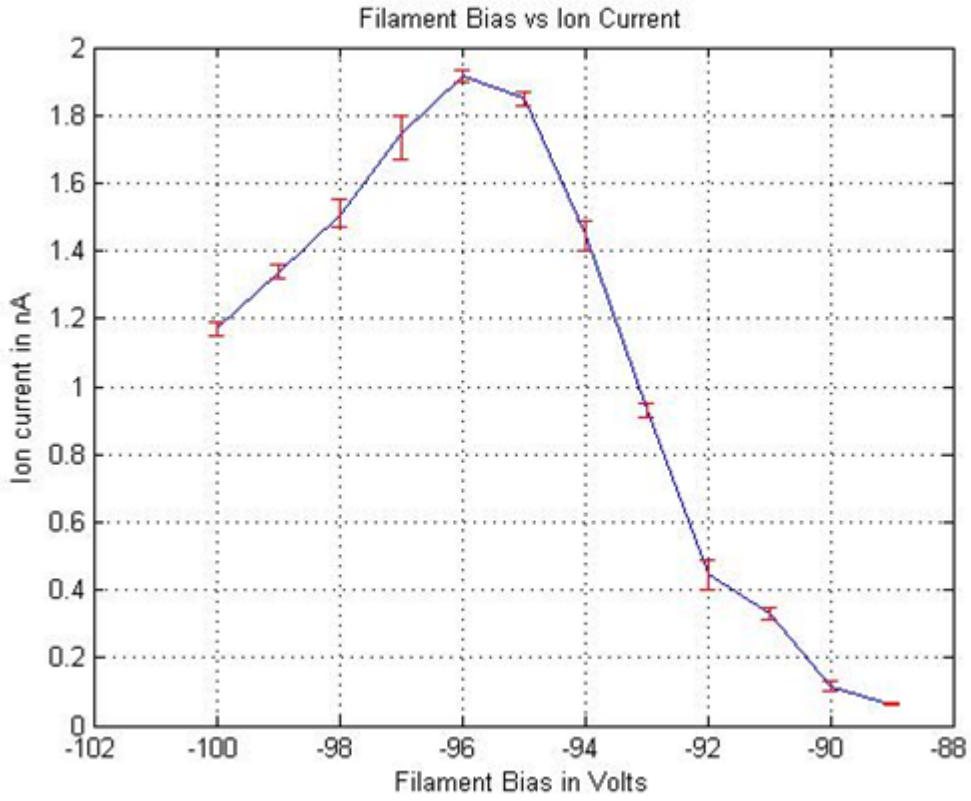

Figure 5.5: Ion Current vs Filament Bias

Since the chamber walls are at -100V, it makes sense that electron emission drops as the filament bias gets closer to -100V due to change in trajectory of emitted electrons (which shifts the area of ionization). On the other hand, higher potential difference between the grid and the filament drives the electron emission higher. These two competing factors make the electron emission peak around -96 V, leading to the observed variation in the ion output current, as shown in the Figure 5.5.

5.3.4 Effect of Grid Bias on output ion current with emissions from a single filament

To measure the effect of grid bias on the output ion current, the grid bias was changed while keeping other biases constant at

- Chamber bias = - 100V
- Filament = - 95 V
- Focus ring = - 40 V
- Repeller = 30 V

the result is shown in Figure 5.6:

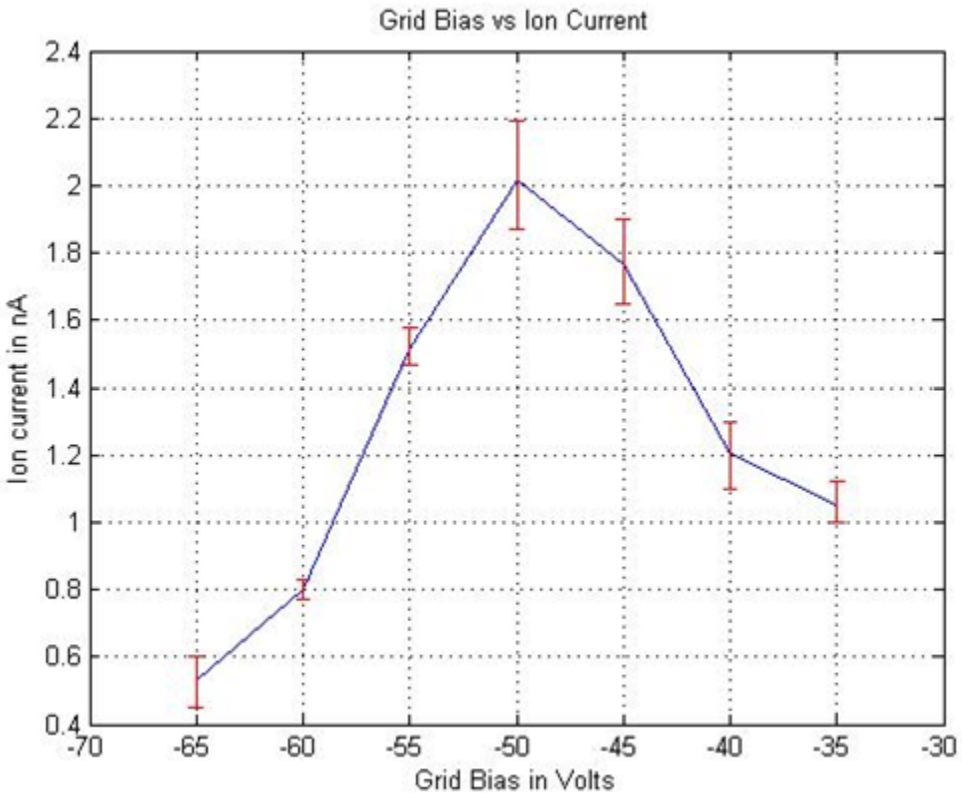

Figure 5.6: Grid Bias vs Ion Current

As seen in the case of changing filament bias, the higher potiential difference between the grid and the filament corresponds to higher electron emission. However, the potential difference between the repeller and the grid varies as well. This changes the area of ionization which in turn has an effect on the output ion current. These two factors make the ion current peak at a grid bias near -50 V.

5.3.5 Effect of Chamber Bias on output ion current with emissions from a single filament

To measure the effect of chamber bias on the output ion current, the chamber bias was changed while keeping other biases constant at

- Grid = - 50 V
- Filament = - 95 V
- Focus ring = - 40 V
- Repeller = 30 V

Figure 5.7 shows the results:

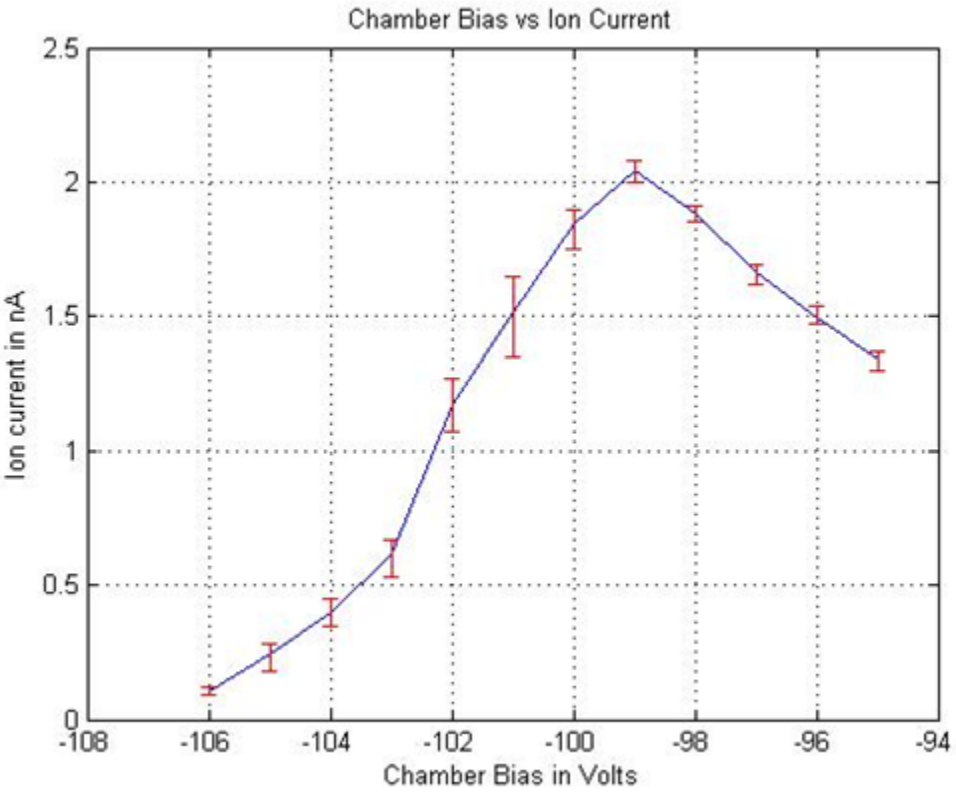

Figure 5.7: Chamber Bias vs Ion Current

The potential difference between the filament and the chamber is important. If the chamber has a higher potential than the filaments, the electrons produced by the filaments will collect on the chamber walls, lowering the number of electrons that reach the region of ionization. The chamber bias can also alter the electron trajectories and affect the volume in which ionization occurs. With these competing factors, the ion current production in the source peaks at around -95 V.

5.3.6 Effect of Repeller Bias on output ion current with emissions from a single filament

Like the previous cases, everything except the repeller bias is kept constant to see the effect of repeller bias on the ion current. The constant biases were :

- Grid = - 50 V
- Filament = - 95 V
- Focus ring = - 40 V
- Chamber bias = - 100V

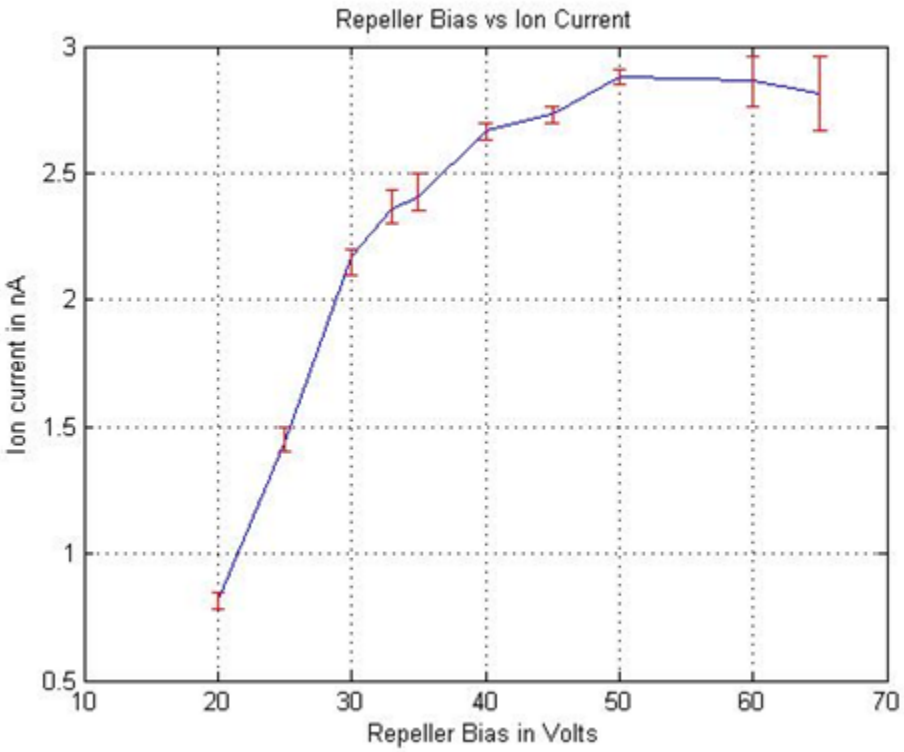

Figure 5.8: Repeller Bias vs Ion Current

Change in repeller bias most likely affects the space charge phenomenon, which in turn modifies the electron and ion trajectories inside the ion source. This leads to the response shown in Figure 5.8:

5.3.7 Effect of Focus Ring Bias on output ion current with emissions from a single filament

To measure the effect of the focus ring bias on the output ion current, the ring bias was changed while keeping other biases constant at

- Grid = - 50 V
- Filament = - 95 V
- Chamber bias = - 100V
- Repeller bias = 30 V

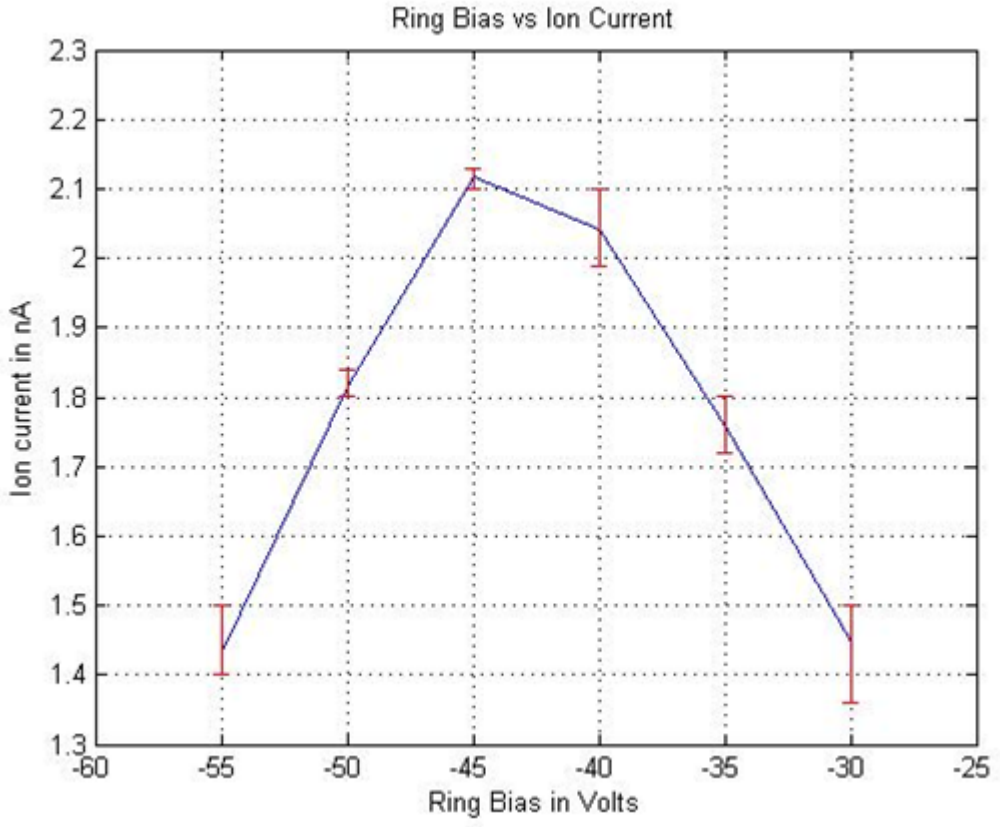

Figure 5.9: Focus Ring Bias vs Ion Current

If the focus ring is at a higher potential than the grid, it collects some of the electrons that are supposed to go towards the repeller. If the focus ring is more negative than the grid the electron trajectories are distorted, causing them to impact the repeller farther from the central axis and the aperture. At the same time, the ring potential must be low enough to attract the ions created inside the source. Figure 5.9 shows the empirical results that arise from these competing factors.

With our mechanical set-up we cannot measure the particle trajectories inside the ion source, so the foregoing attempt to rationalize the effects of surface biases are mere conjectures. All the above results are shown for emission from a single filament and the results might change when emissions from multiple filaments are introduced. Accurate quantification of the space charging effects and the effect of electron emission trajectories on each other is beyond the scope of this study but is a valid endeavor for future work. The above conclusions represent the most likely scenarios that can explain the results shown.

5.4 Tuning the biases to obtain useful emission

Once the effects of all ion source surfaces are known, the knowledge was used to maximize the ion source output. The combination that yeilded maximum ion current production was:

- Grid = - 50 V
- Filmanet = - 95 V
- Focus ring = - 40 V
- Chamber bias = - 100V
- Repeller Bias = 70 V

The ion output current was about 4 nA from the emission of one filament.

5.5 Superposition of two filaments

Once results were seen from one filament, two filaments were used to see if the results doubled. Electron currents to the repeller and the grid were also measured, along with the ion current, for both single and double filaments.

The results are documented in the Table below:

Case	Filament #1	Filament#2	Filament#1 + Filament#2
Emission	1420 μA	1310 μA	
Repeller	1100 μA	1000 μA	$\sim$ 2000 μA
Grid	280 μA	290 μA	$\sim$ 500 μA
Ion Output	$\sim$ 4 nA	$\sim$ 3.5 nA	>7 nA

Table 5.1: Superposition of two filaments

The results obtained suggest that superpostion takes place approximately as expected, with only small departures from linearity.

Chapter 6

Conclusions and future work

This thesis describes and characterizes a new laboratory-based source design that can simulate conditions similar to the ionosphere at LEO altitudes. These conditions can then be used to calibrate/test space-borne instruments. The control electronics that drive the filaments and provide biases to different surfaces inside the source are discussed in great detail. The ion source electronics were designed to be modular, and can be used for other projects that require filament emission control or need programmable surface biases. This document also provides the details of the software used. A simple yet robust controller was used to control the emission currents from all filaments.

As per the requirements laid out in Chapter 2, Ionsim produces minimal photon flux at the output. Since the characterization curves (Figure 5.5 - Figure 5.9) have reasonable error bars, we can deduce that the results are repeatable. The Ionsim control software takes serial commands as input and can therefore be controlled by user generated serial instructions from a LabView interface.

Based on the ion densities in Table 2.1, an RPA[8] with an aperture of radius 0.038m and flying at a height of 400 km is expected to receive ion flux corresponding to 0.27 μA (midnight) to 0.52 μA (noon) ion current. Minimum current measured by RPAs is 10 times the

noise level (∼100pA), or 1 nA. The ion source can generate ion current of about 20 nA at 4×10^{-5} torr neutral pressure which is more than 1nA. Moreover, as shown in Figure 5.4, the neutral pressure can be increased to maximize the output ion flux and cover more of the range expected by an RPA at this altitude.

Although we are unable to measure the mean energy of the ion beam produced by the source, the Ion-optics simulation (Figure 2.6) which was the basis of all experiments provided an ion beam with a mean energy of 7 eV. Since the final optimized surface biases were not too far off from the initial guess, it can be hypothesized that the mean energy of the ion beam is about 7eV. This is comparable to the mean ion energy that an instrument is expected to encounter at LEO. Moreover, since the source potential can be floated relative to the space-borne instruments that are to be tested, it is possible to adjust the mean energy of the ion beam. The ion composition in LEO can be reproduced if a vacuum chamber could provide the source with atomic oxygen. Since that is not possible, the source can use any other species (in our case, nitrogen) to generate ion beam with mean energy that is equivalent to atomic oxygen ions at LEO altitudes.

Various optimizations and changes need to be made to make IonSim a finalized product. There is no dearth of future work to be done. The list below provides possible and non-comprehensive improvements to the study described in this thesis:

- The ion energy distributions of the output ion beam need to be characterized using a retarding potential analyzer (RPA).
- The spread of the ion beam at various distances from the aperture of the source can be characterized using a beam imager.
- While the simple one-bit integrator controller works well in controlling electron emissions, a PID controller scheme combined with a model reference adaptive control (MRAC) to autotune the controller parameters which react to changing filament resistance might allow more precise control of the ion beam.

- The characterization of the ion source presented here was done with emission from a single filament. This can be expanded upon and effects of emissions from multiple filaments can be studied in details. This would be a better representation of the final product, and would include the effects of space charge due to multiple filaments operating simultaneously.

- Using the data points generated during the characterization study of the source, a neural network could be trained to produce ion emissions with particular mean velocities and temperatures.

- The cost effectiveness of the design can be improved by separating the digital control from the analog drivers and using opto-isolators instead of isolation amplifiers. While this would lead to cheaper system, it will involve a significant redesign effort.

Appendix A

The Voltage Regulator Board Schematics

This appendix section includes:

1. Schematic of the Voltage regulated board that provides positive bias to the repeller;
2. Schematic of the Voltage regulated boards that provides negative bias to the filaments and the chamber;
3. Schematic of the Voltage regulated boards containing dual DC-DC converters that provides negative bias to the grid and the focus ring;

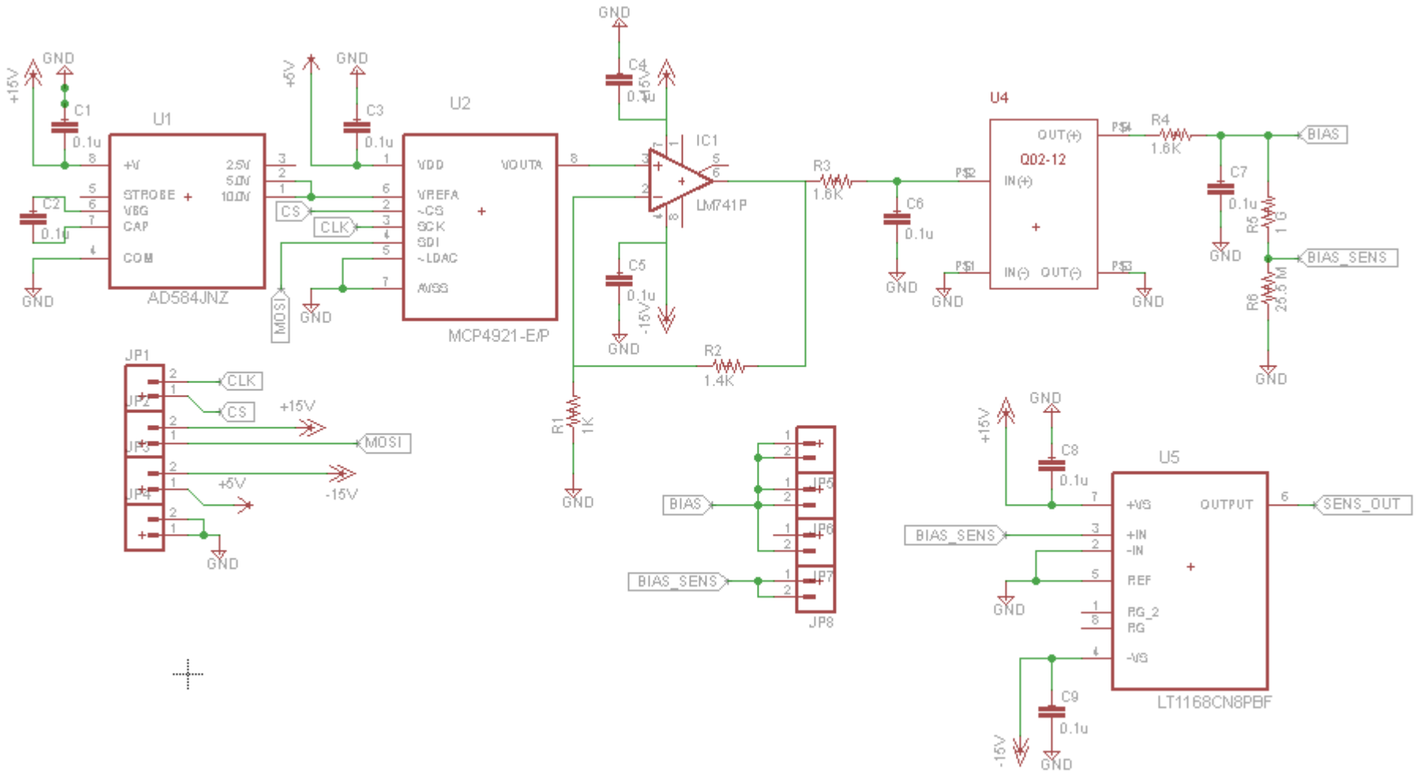

Figure A.1: Schematic of the Voltage regulated board that provides positive bias to the repeller

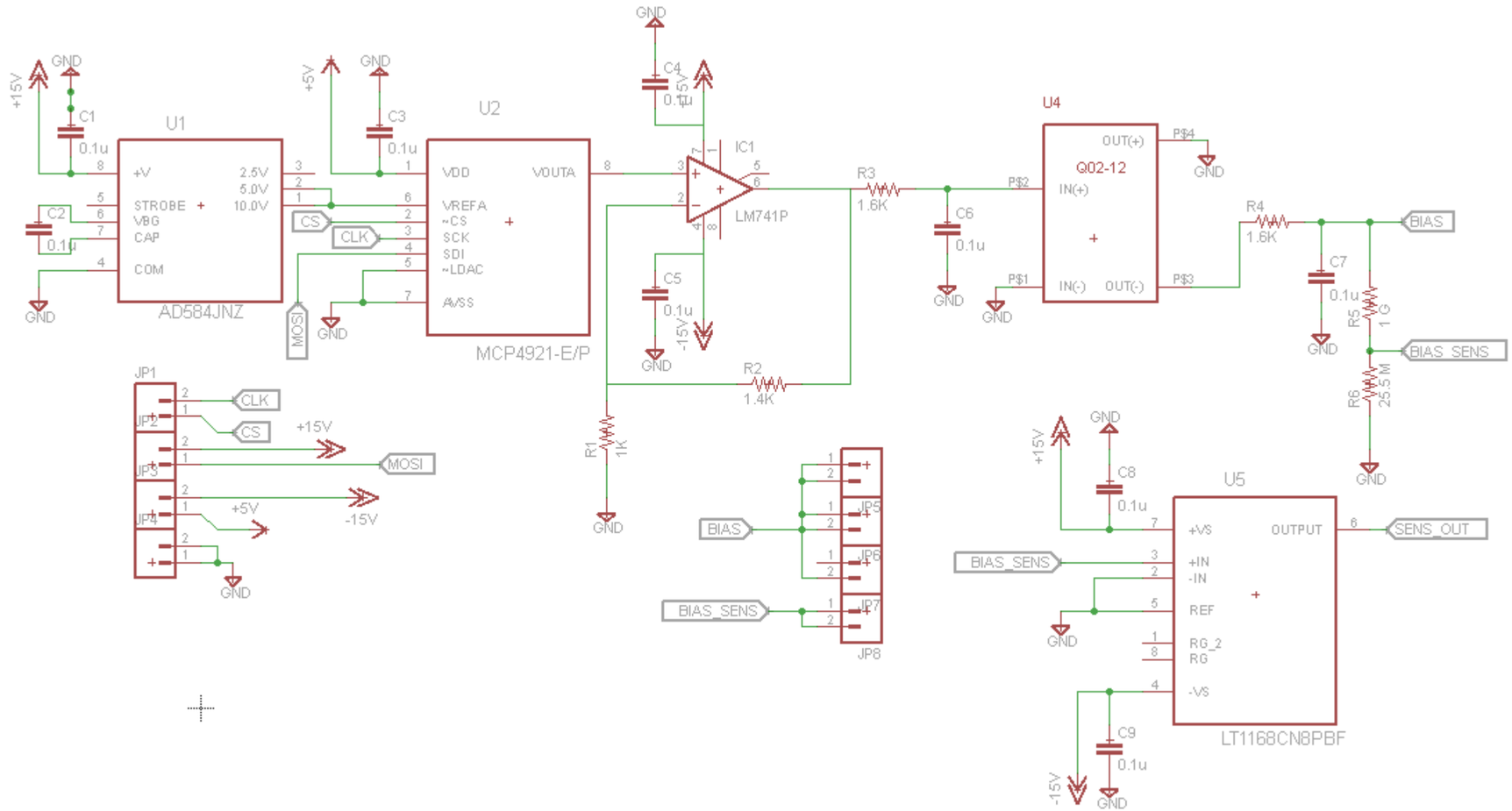

Figure A.2: Schematic of the Voltage regulated boards that provides negative bias to the filaments and the chamber

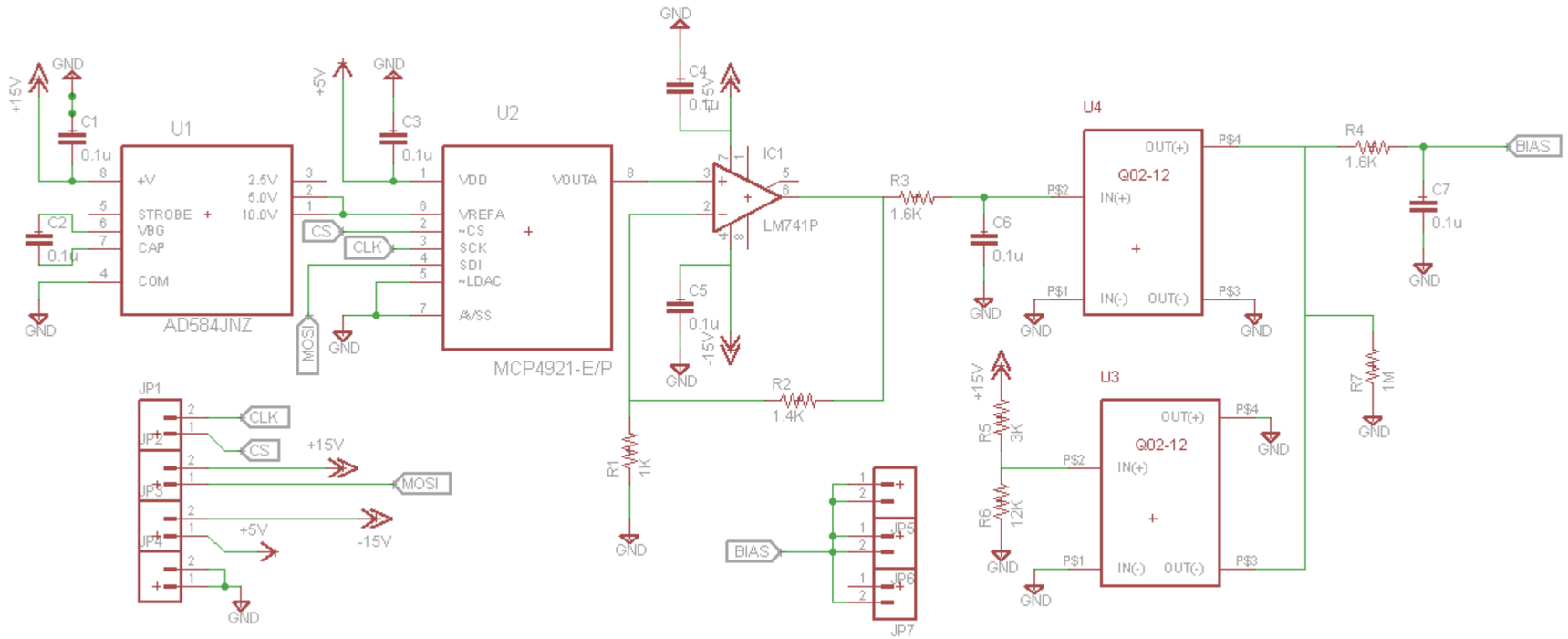

Figure A.3: Schematic of the Voltage regulated boards containing dual DC-DC converters that provides negative bias to the grid and the focus ring

Appendix B

The Filament Driver Board Schematic

This appendix section includes a schematic of a filament driver board. This board only performs the basic function of driving the filament and sensing filament and the emission current. Advanced features such as:

1. Digital control of output current limit to protect filaments from overheating;
2. Optocouplers (4938s) and N channel CMOS to monitor the E/S pins for thermal shut-down
3. A circuit for driving the E/S pin to logic low for disabling the current output of the power amplifier.

are not included in this version.

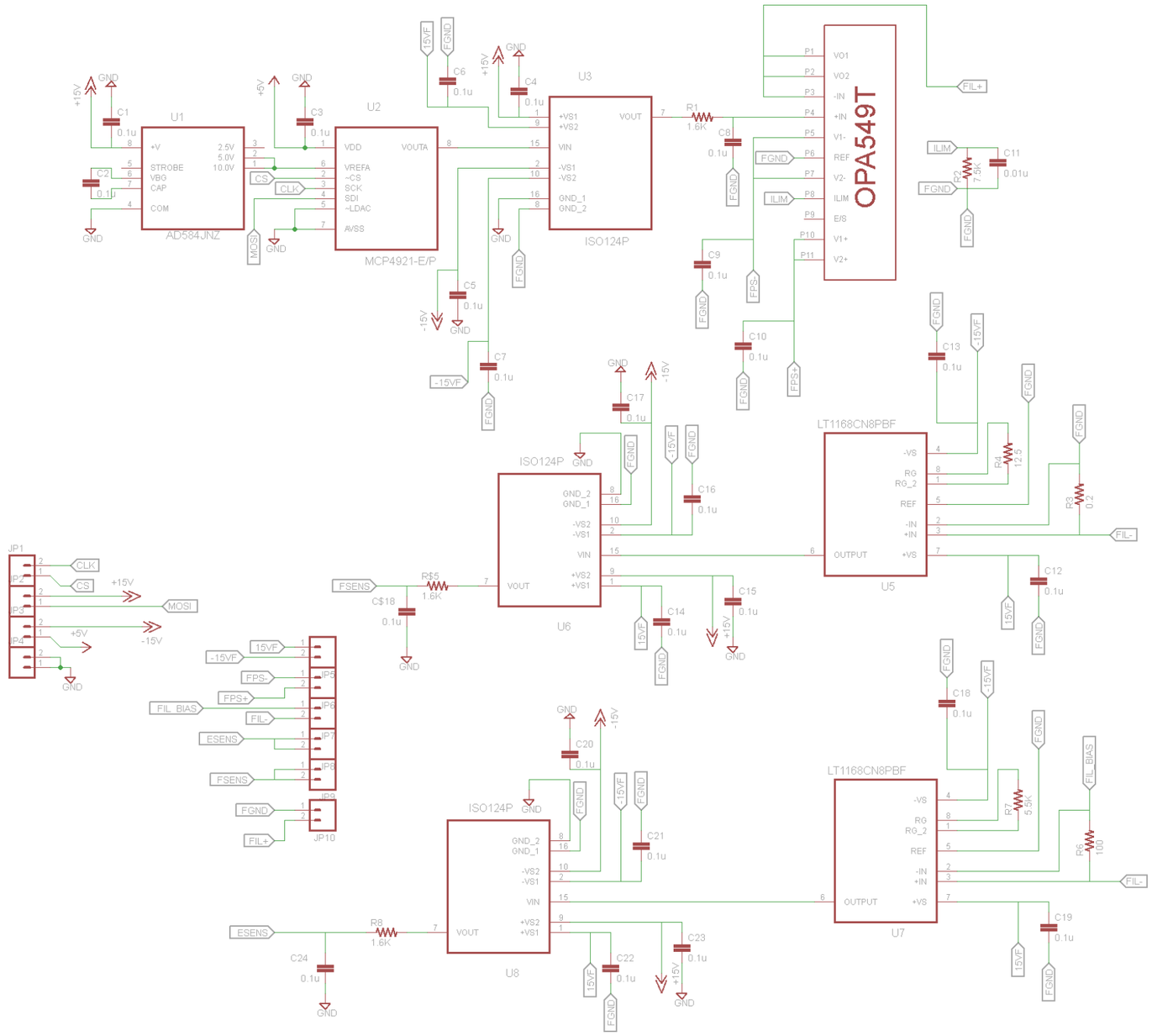

Figure B.1: Schematic of the Voltage regulated board that provides positive bias to the repeller

Appendix C

Embdedded software

```
#include "SPI.h"

word outputValue = 0;
byte data = 0;

const int NUMBER_OF_FIELDS = 3;
int fieldIndex = 0;
int values[NUMBER_OF_FIELDS];

int board;
int channel;
int control;

// filament control channels
int fila = 5;
```

```
  int filb = 6;
  int filc = 7;
  int fild = 8;

  // filament inputs
  int valuea = 1;
  int valueb = 2;
  int valuec = 3;
  int valued = 4;

  //computational variables
  int input;

  //delay between reading for average
  int time = 1; // 1ms

  // filament current limit
  int limit = 2000;

void setup()
  {
      // voltage control pins
      pinMode(10, OUTPUT); //repeller
      pinMode(2, OUTPUT); // chamber
      pinMode(3, OUTPUT); // filament
      pinMode(4, OUTPUT);  // focusring
       pinMode(5, OUTPUT);  // grid
```

```
    //filament control pins
    pinMode(6, OUTPUT);
    pinMode(7, OUTPUT);
    pinMode(8, OUTPUT);
    pinMode(9, OUTPUT);

    SPI.begin();
    SPI.setBitOrder(MSBFIRST);
    Serial.begin(9600);
  }

void loop()
  {
   if (Serial.available())
     {
      char ch = Serial.read();
      if(ch >= '0' && ch <= '9')
      {
        if(fieldIndex < NUMBER_OF_FIELDS)
          {
             values[fieldIndex] = (values[fieldIndex] * 10) + (ch - '0');
          }
      }
      else if (ch == ',')
      {
        fieldIndex++; // increment field index
      }
```

```
else
{
   board = values[0];
   channel = values[1];
   control = values[2];

      if (board ==1)//voltage boards
      {
        Serial.println("voltage board");
        calibration (channel);
        if (control < 4095){
            set(channel,control);
          }
        else{
            set(channel,4095);
        }
      } // end voltageboards

      if (board ==2) // filament boards
      {
        Serial.println("filament board");
       // filament 1
        controller(fila, valuea, control);
       // filament 2
        controller(filb, valueb, control);
       // filament 3
        controller(filc, valuec, control);
       // filament 4
```

```
            controller(fild, valued, control);
          } // end filament board

          values[0] = 0;
          values[1] = 0;
          values[2] = 0;

          fieldIndex = 0;
      }

  } // end if serial availale
 } // end loop


 void set(int pin, int value)
   {
       outputValue = value;
       digitalWrite(pin, LOW);
       data = highByte(outputValue);
       data = 0b00001111 & data;
       data = 0b00110000 | data;
       SPI.transfer(data);
       data = lowByte(outputValue);
       SPI.transfer(data);
       digitalWrite(pin, HIGH);
   }

void controller(int controlpin, int inputpin, int control)
```

```
{
    input = 0;
    for (int i = 0; i < 5; i++) {
      input = input + analogRead(inputpin);
      delay(time);
    }// end for loop
    input = input/5; // moving average

if (input < control) outputValue = outputValue+1;
if (input > control) outputValue = outputValue-1;

if (outputValue < limit)
  {
      digitalWrite(controlpin, LOW);
      data = highByte(outputValue);
      data = 0b00001111 & data;
      data = 0b00110000 | data;
      SPI.transfer(data);
      data = lowByte(outputValue);
      SPI.transfer(data);
      digitalWrite(controlpin, HIGH);
  }
 else {
      digitalWrite(controlpin, LOW);
      data = highByte(limit);
      data = 0b00001111 & data;
      data = 0b00110000 | data;
      SPI.transfer(data);
```

```
        data = lowByte(limit);
        SPI.transfer(data);
        digitalWrite(controlpin, HIGH);
    }

  }

  void calibration (int pin)
  {
    for (int i = 0; i < 5; i++) {
      outputValue = 0;
      digitalWrite(pin, LOW);
      data = highByte(outputValue);
      data = 0b00001111 & data;
      data = 0b00110000 | data;
      SPI.transfer(data);
      data = lowByte(outputValue);
      SPI.transfer(data);
      digitalWrite(pin, HIGH);
      delay(1000);
    }
  }
```

Bibliography

[1] Microchip. MCP4901/4911/4921 8/10/12-Bit Voltage Output D/A Converter w/ SPI.

[2] Kanu, A. B., Dwivedi, P., Tam, M., Matz, L., and Jr, H. H. H., 2008. "Ion mobility - mass spectrometry". *Journal of Mass Spectrometry,* ***43***, pp. 1–22.

[3] Yates, J. R., Ruse, C. I., and Nakorchevsky, A., 2009. "Proteomics by mass spectrometry: approaches, advances, and applications.". In Annual review of biomedical engineering, Vol. 11, pp. 49–79.

[4] Moak, C., Banta, H., Thurtson, J., Johnson, J., and King, R., 1959. "Duo Plasmatron Ion Source for Use in Accelerators". *Review of Scientific Instruments,* ***30***(8), pp. 694–699.

[5] Kaufman, H., 1961. An ion rocket with an electron-bombardment ion source. Tech. rep., National Aeronautics and Space Administration. Lewis Research Center, Cleveland.

[6] Filjari, R., Kosi, T., and Markezic, I., 2006. "GPS Ionospheric Error Correction Models". In 48th International Symposium ELMAR-2006, no. June, pp. 7–9.

[7] Hernández-Pajares, M., Juan, J. M., Sanz, J., Aragón-Àngel, A., García-Rigo, A., Salazar, D., and Escudero, M., 2011. "The ionosphere: effects, GPS modeling and the benefits for space geodetic techniques". *Journal of Geodesy,* ***85***(12), Sept., pp. 887–907.

[8] Hanson, W. B., Heelis, R. A., Power, R. A., Lippincott, C. R., Zuccaro, D. R., Holt,

B. J., Harmon, L. H., and Sanatani, S., 1982. "The Retarding Potential Analyzer for Dynamics Explorer-B". *Space Science Instrumentation,* ***5***, pp. 503–510.

[9] March, R. E., and Todd, J. F. J., 1995. *Practical Aspects of Ion Trap Mass Spectrometry: Fundamentals of Ion Trap Mass Spectrometry.* CRC Press.

[10] Heelis, R. A., Hanson, W. B., Lippincott, C. R., Zuccaro, D. R., Harmon, L. H., Holt, B. J., Doherty, J. E., and Power, R. A., 1982. "The Ion Drift Meter for Dynamics Explorer-B". *Space Science Instrumentation,* ***5***, pp. 511–521.

[11] Knudsen, W. C., Spenner, K., Bakke, J., and Novak, V., 1980. "Pioneer Venus Orbiter Planar Retarding Potential Analyzer Plasma Experiment". *IEEE Transactions on Geoscience and Remote Sensing.*

[12] Cragin, B. L., Hanson, W. B., and Sanatani, S., 1982. "The solar wind interaction with Mars as seen by the Viking retarding potential analyzers". *Journal of Geophysical Research,* ***87***, pp. 4395–4404.

[13] Iwata, T., 1988. "Photon stimulated gas desorption from pure aluminum". *Journal of Vacuum Science & Technology A: Vacuum, Surfaces, and Films,* ***6***(3), May, p. 1297.

[14] Lulai, P., 2001. Determination of filament work function in vacuum. Tech. rep., AVS.

[15] Davidson, R. L., 2011. "Grid geometry based errors in retarding potential analyzer measurements". PhD thesis.

[16] Analog Devices. AD584 Data Sheet Rev C.

[17] Texas Instruments. OPA548: High-Voltage, High-Current Operational Amplifier (Rev. B).

[18] EMCO High Voltage Corporation. Q SERIES Datasheet.

[19] Linear Technology. LT1168 - Low Power, Single Resistor Gain Programmable, Precision Instrumentation Amplifier.

[20] Atmel. ATmega640/1280/1281/2560/2561 Complete datasheet.

[21] EMCO High Voltage Corporation, 2012. Impact of Source Resistance on EMCO High Voltage Converters.

[22] Burr-Brown. OPA549 -High-Voltage, High-Current OPERATIONAL AMPLIFIER.

[23] Flaxer, E., 2011. "Programmable smart electron emission controller for hot filament.". *The Review of scientific instruments,* ***82***(2), Feb., p. 025111.

[24] Burr-Brown. IS0124-Precision Lowest-Cost ISOLATION AMPLIFIER.

[25] Cooper, D. J. *Practical Process Control:Proven Methods and Best Practices for Automatic PID Control.*